ISSN 1949-8470 (online)

World Journal of *Radiology*

World J Radiol 2017 January 28; 9(1): 1-26

Published by Baishideng Publishing Group Inc

WJR World Journal of Radiology

A peer-reviewed, online, open-access journal of Radiology

Editorial Board

2014-2017

The *World Journal of Radiology* Editorial Board consists of 365 members, representing a team of worldwide experts in radiology. They are from 36 countries, including Afghanistan (1), Argentina (2), Australia (5), Austria (7), Belgium (2), Brazil (8), Canada (6), Chile (1), China (43), Croatia (1), Denmark (4), Egypt (6), France (5), Germany (22), Greece (10), India (12), Iran (6), Ireland (2), Israel (3), Italy (47), Japan (13), Netherlands (1), New Zealand (1), Pakistan (1), Poland (2), Portugal (1), Serbia (1), Singapore (3), Slovakia (1), South Korea (18), Spain (4), Sweden (2), Switzerland (4), Thailand (1), Turkey (26), United Kingdom (11), and United States (82).

Yue-Qi Zhu, *Shanghai*

Croatia

Goran Kusec, Osijek

Denmark

Poul E Andersen, *Odense*
Lars J Petersen, *Aalborg*
Thomas Z Ramsoy, *Frederiksberg*
Morten Ziebell, *Copenhagen*

Egypt

Mohamed F Bazeed, *Mansoura*
Mohamed Abou El-Ghar, *Mansoura*
Reem HA Mohamed, *Cairo*
Mohamed R Nouh, *Alexandria*
Ahmed AKA Razek, *Mansoura*
Ashraf A Zytoon, *Shebin El-Koom*

France

Sabine F Bensamoun, *Compiègne*
Romaric Loffroy, *Dijon*
Stephanie Nougaret, *Montpellier*
Hassane Oudadesse, *Rennes*
Vincent Vinh-Hung, *Fort-de-France*

Germany

Henryk Barthel, *Leipzig*
Peter Bannas, *Hamburg*
Martin Beeres, *Frankfurt*
Ilja F Ciernik, *Dessau*
A Dimitrakopoulou-Strauss, *Heidelberg*
Peter A Fasching, *Erlanegn*
Andreas G Schreyer, *Regensburg*
Philipp Heusch, *Duesseldorf*
Sonja M Kirchhoff, *Munich*
Sebastian Ley, *Munich*
Adel Maataoui, *Frankfurt am Main*
Stephan M Meckel, *Freiburg*
Hans W Muller, *Duesseldorf*
Kay Raum, *Berlin*
Dirk Rades, *Luebeck*
Marc-Ulrich Regier, *Hamburg*
Alexey Surov, *Halle*
Martin Walter, *Magdeburg*
Axel Wetter, *Essen*
Christoph Zilkens, *Düsseldorf*

Greece

Panagiotis Antoniou, *Thessaloniki*
Nikos Efthimiou, *Athens*
Dimitris Karnabatidis, *Patras*
George Latsios, *Athens*
Stylianos Megremis, *Iraklion*
Alexander D Rapidis, *Athens*
Kiki Theodorou, *Larissa*
Ioannis A Tsalafoutas, *Athens*
Evanthia E Tripoliti, *Ioannina*
Athina C Tsili, *Ioannina*

India

Ritesh Agarwal, *Chandigarh*
Chandan J Das, *New Delhi*
Prathamesh V Joshi, *Mumbai*
Naveen Kalra, *Chandigarh*
Chandrasekharan Kesavadas, *Trivandrum*
Jyoti Kumar, *New Delhi*
Atin Kumar, *New Delhi*
Kaushala P Mishra, *Allahabad*
Daya N Sharma, *New Delhi*
Binit Sureka, *New Delhi*
Sanjay Sharma, *New Delhi*
Raja R Yadav, *Allahabad*

Iran

Majid Assadi, *Bushehr*
SeyedReza Najafizadeh, *Tehran*
Mohammad Ali Oghabian, *Tehran*
Amir Reza Radmard, *Tehran*
Ramin Sadeghi, *Mashhad*
Hadi Rokni Yazdi, *Tehran*

Ireland

Tadhg Gleeson, *Wexford*
Frederik JAI Vernimmen, *Cork*

Israel

Dafna Ben Bashat, *Tel Aviv*
Amit Gefen, *Tel Aviv*
Tamar Sella, *Jerusalem*

Italy

Adriano Alippi, *Rome*
Dante Amelio, *Trento*
Michele Anzidei, *Rome*
Filippo F Angileri, *Messinas*
Stefano Arcangeli, *Rome*
Roberto Azzoni, *San Donato milanese*
Tommaso V Bartolotta, *Palermo*
Tommaso Bartalena, *Imola*
Livia Bernardin, *San Bonifacio*
Federico Boschi, *Verona*
Sergio Casciaro, *Lecce*
Emanuele Casciani, *Rome*
Musa M Can, *Napoli*
Alberto Cuocolo, *Napoli*
Michele Ferrara, *Coppito*
Mauro Feola, *Fossano*
Giampiero Francica, *Castel Volturno*
Luigi De Gennaro, *Rome*
Giulio Giovannetti, *Pisa*
Francesca Iacobellis, *Napoli*
Formato Invernizzi, *Monza Brianza*
Francesco Lassandro, *Naples*
Lorenzo Livi, *Florence*
Pier P Mainenti, *Napoli*
Laura Marzetti, *Chieti*
Giuseppe Malinverni, *Crescentino*
Enrica Milanesi, *Turin*
Giovanni Morana, *Treviso*
Lorenzo Monti, *Milan*
Silvia D Morbelli, *Genoa*
Barbara Palumbo, *Perugia*
Cecilia Parazzini, *Milan*
Stefano Pergolizzi, *Messina*
Antonio Pinto, *Naples*
Camillo Porcaro, *Rome*
Carlo C Quattrocchi, *Rome*
Alberto Rebonato, *Perugia*
Giuseppe Rizzo, *Rome*
Roberto De Rosa, *Naples*
Domenico Rubello, *Rovigo*
Andrea Salvati, *Bari*
Sergio Sartori, *Ferrara*
Luca M Sconfienza, *Milano*
Giovanni Storto, *Rionero*
Nicola Sverzellati, *Parma*
Alberto S Tagliafico, *Genova*
Nicola Troisi, *Florence*

Japan

Yasuhiko Hori, *Chiba*
Hidetoshi Ikeda, *Koriyama*
Masahito Kawabori, *Sapporo*
Tamotsu Kamishima, *Sapporo*
Hiro Kiyosue, *Yufu*
Yasunori Minami, *Osaka-sayama*
Yasuhiro Morimoto, *Kitakyushu*
Satoru Murata, *Tokyo*
Shigeki Nagamachi, *Miyazaki*
Hiroshi Onishi, *Yamanashi*
Morio Sato, *Wakayama Shi*
Yoshito Tsushima, *Maebashi*
Masahiro Yanagawa, *Suita*

Netherlands

Willem Jan van Rooij, *Tilburg*

New Zealand

W Howell Round, *Hamilton*

Pakistan

Wazir Muhammad, *Abbottabad*

Poland

Maciej S Baglaj, *Wroclaw*

Piotr Czauderna, *Gdansk*

Portugal

Joao Manuel RS Tavares, *Porto*

Serbia

Olivera Ciraj-Bjelac, *Belgrade*

Singapore

Gopinathan Anil, *Singapore*
Terence KB Teo, *Singapore*
Cher Heng Tan, *Singapore*

Slovakia

Stefan Sivak, *Martin*

South Korea

Ki Seok Choo, *Busan*
Seung Hong Choi, *Seoul*
Dae-Seob Choi, *Jinju*
Hong-Seok Jang, *Seoul*
Yong Jeong, *Daejeon*
Chan Kyo Kim, *Seoul*
Se Hyung Kim, *Seoul*
Joong-Seok Kim, *Seoul*
Sang Eun Kim, *Seongnam*
Sung Joon Kwon, *Seoul*
Jeong Min Lee, *Seoul*
In Sook Lee, *Busan*
Noh Park, *Goyang*
Chang Min Park, *Seoul*
Sung Bin Park, *Seoul*
Deuk Jae Sung, *Seoul*
Choongsoo Shin, *Seoul*
Kwon-Ha Yoon, *Iksan*

Spain

Miguel A De Gregorio, *Zaragoza*
Antonio Luna, *Jaén*
Enrique Marco de Lucas, *Santander*
Fernando Ruiz Santiago, *Granada*

Sweden

Dmitry Grishenkov, *Stockholm*
Tie-Qiang Li, *Stockholm*

Switzerland

Nicolau Beckmann, *Basel*
Christian Boy, *Bern*
Giorgio Treglia, *Bellinzona*

Stephan Ulmer, *Kiel*

Thailand

Sirianong Namwongprom, *Chiang Mai*

Turkey

Kubilay Aydin, *Istanbul*
Ramazan Akdemir, *Sakarya*
Serhat Avcu, *Ankara*
Ayse Aralasmak, *Istanbul*
Oktay Algin, *Ankara*
Nevbahar Akcar, *Meselik*
Bilal Battal, *Ankara*
Zulkif Bozgeyik, *Elazig*
Nazan Ciledag, Aakara
Fuldem Y Donmez, *Ankara*
Gulgun Engin, *Istanbul*
Ahmet Y Goktay, *Izmir*
Oguzhan G Gumustas, *Bursa*
Kaan Gunduz, *Ankara*
Pelin Ozcan Kara, *Mersin*
Kivanc Kamburoglu, *Ankara*
Ozgur Kilickesmez, *Istanbul*
Furuzan Numan, *Istanbul*
Cem Onal, *Adana*
Ozgur Oztekin, *Izmir*
Seda Ozbek (Boruban), *Konya*
Selda Sarikaya, *Zonguldak*
Figen Taser, *Kutahya*
Baran Tokar, *Eskisehir*
Ender Uysal, *Istanbul*
Ensar Yekeler, *Istanbul*

United Kingdom

Indran Davagnanam, *London*
M DC Valdés Hernández, *Edinburgh*
Alan Jackson, *Manchester*
Suneil Jain, *Belfast*
Long R Jiao, *London*
Miltiadis Krokidis, *Cambridge*
Pradesh Kumar, *Liverpool*
Peter D Kuzmich, *Derby*
Georgios Plataniotis, *Brighton*
Vanessa Sluming, *Liverpool*

United States

Garima Agrawal, *Saint Louis*
James R Brasic, *Baltimore*
Rajendra D Badgaiyan, *Buffalo*
Ulas Bagci, *Bethesda*
Anat Biegon, *Stony Brook*
Ramon Casanova, *Winston Salem*
Wenli Cai, *Boston*
Zheng Chang, *Durham*
Corey J Chakarun, *Long Beach*
Kai Chen, *Los Angeles*
Hyun-Soon Chong, *Chicago*
Marco Cura, *Dallas*
Ravi R Desai, *Bensalem*
Delia DeBuc, *Miami*
Carlo N De Cecco, *Charleston*
Timm-Michael L Dickfeld, *Baltimore*
Subba R Digumarthy, *Boston*
Huy M Do, *Stanford*
Todd A Faasse, *Grand Rapids*
Salomao Faintuch, *Boston*
Girish M Fatterpekar, *New York*
Dhakshinamoorthy Ganeshan, *Houston*
Robert J Griffin, *Little Rock*
Andrew J Gunn, *Boston*
Sandeep S Hedgire, *Boston*
Timothy J Hoffman, *Columbia*
Mai-Lan Ho, *San Francisco*
Juebin Huang, *Jackson*
Abid Irshad, *Charleston*
Matilde Inglese, *New York*
El-Sayed H Ibrahim, *Jacksonville*
Paul R Julsrud, *Rochester*
Pamela T Johnson, *Baltimore*
Ming-Hung Kao, *Tempe*
Sunil Krishnan, *Houston*
Richard A Komoroski, *Cincinnati*
Sandi A Kwee, *Honolulu*
King Kim, *Ft. Lauderdale*
Guozheng Liu, *Worcester*
Yiyan Liu, *Newark*
Venkatesh Mani, *New York*
Lian-Sheng Ma, *Pleasanton*
Rachna Madan, *Boston*
Zeyad A Metwalli, *Houston*
Yilong Ma, *Manhasset*
Hui Mao, *Atlanta*
Feroze B Mohamed, *Philadelphia*
Gul Moonis, *Boston*
John L Nosher, *New Brunswick*
Rahmi Oklu, *Boston*
Aytekin Oto, *Chicago*
Bishnuhari Paudyal, *Philadelphia*
Rajul Pandya, *Youngstown*
Chong-Xian Pan, *Sacramento*
Jay J Pillai, *Baltimore*
Neal Prakash, *Duarte*
Reza Rahbar, *Boston*
Ali S Raja, *Boston*
Gustavo J Rodriguez, *El Paso*
David J Sahn, *Portlsand*
Steven Schild, *Scottsdale*
Ali R Sepahdari, *Los Angeles*
Li Shen, *Indianapolis*
JP Sheehan, *Charlottesville*
Atul B Shinagare, *Boston*
Sarabjeet Singh, *Boston*
Charles J Smith, *Columbia*
Kenji Suzuki, *Chicago*
Monvadi Srichai-Parsia, *Washington*
Sree H Tirumani, *Boston*
Hebert A Vargas, *New York*
Sachit Verma, *Philadelphia*
Yoichi Watanabe, *Minneapolis*
Li Wang, *Chapel Hill*
Carol C Wu, *Boston*
Shoujun Xu, *Houston*
Min Yao, *Cleveland*
Xiaofeng Yang, *Atlanta*
Qingbao Yu, *Albuquerque*
Aifeng Zhang, *Chicago*
Chao Zhou, *Bethlehem*
Hongming Zhuang, *Philadelphia*

WJR World Journal of Radiology

Contents

Monthly Volume 9 Number 1 January 28, 2017

Contents

World Journal of Radiology
Volume 9 Number 1 January 28, 2017

NAME OF JOURNAL
World Journal of Radiology

ISSN
ISSN 1949-8470 (online)

LAUNCH DATE
January 31, 2009

FREQUENCY
Monthly

EDITORIAL OFFICE
Xiu-Xia Song, Director
World Journal of Radiology
Baishideng Publishing Group Inc
8226 Regency Drive, Pleasanton, CA 94588, USA
Telephone: +1-925-2238242
Fax: +1-925-2238243
E-mail: editorialoffice@wjgnet.com
Help Desk: http://www.wjgnet.com/esps/helpdesk.aspx
http://www.wjgnet.com

PUBLISHER
Baishideng Publishing Group Inc
8226 Regency Drive,
Pleasanton, CA 94588, USA
Telephone: +1-925-2238242
Fax: +1-925-2238243
E-mail: bpgoffice@wjgnet.com
Help Desk: http://www.wjgnet.com/esps/helpdesk.aspx
http://www.wjgnet.com

PUBLICATION DATE
January 28, 2017

World Journal of Radiology

Submit a Manuscript: http://www.wjgnet.com/esps/
Help Desk: http://www.wjgnet.com/esps/helpdesk.aspx
DOI: 10.4329/wjr.v9.i1.1

World J Radiol 2017 January 28; 9(1): 1-4
ISSN 1949-8470 (online)

EDITORIAL

Cutting edge clinical applications in cardiovascular magnetic resonance

Carlo N De Cecco, Giuseppe Muscogiuri, Akos Varga-Szemes, U Joseph Schoepf

Carlo N De Cecco, Akos Varga-Szemes, U Joseph Schoepf, Division of Cardiovascular Imaging, Department of Radiology and Radiological Science, Medical University of South Carolina, Charleston, SC 29425, United States

Giuseppe Muscogiuri, Department of Imaging, Bambino Gesù - Children's Hospital IRCCS, 00146 Rome, Italy

Giuseppe Muscogiuri, Department of Clinical and Molecular Medicine, University of Rome "Sapienza", 00185 Rome, Italy

U Joseph Schoepf, Division of Cardiology, Department of Medicine, Medical University of South Carolina, Charleston, SC 29425, United States

Author contributions: De Cecco CN, Muscogiuri G, Varga-Szemes A and Schoepf UJ all contributed equally to conception, drafting the article and revising it critically for intellectual content.

Conflict-of-interest statement: Dr. U Joseph Schoepf is a consultant for and/or receives research support from Astellas, Bayer, Bracco, GE, Guerbet, Medrad, and Siemens; De Cecco is a consultant for Guerbet and receives financial support from Siemens. The other authors declare no conflict of interest.

Manuscript source: Invited manuscript

Correspondence to: Carlo N De Cecco, MD, PhD, Division of Cardiovascular Imaging, Department of Radiology and Radiological Science, Medical University of South Carolina, 25 Courtenay Drive, MSC 226, Charleston, SC 29425, United States. dececco@musc.edu
Telephone: +1-843-8763185
Fax: +1-843-8763157

Received: September 14, 2016
Peer-review started: September 18, 2016
First decision: October 21, 2016
Revised: November 4, 2016
Accepted: November 27, 2016
Article in press: November 29, 2016
Published online: January 28, 2017

Abstract

Today, the use of cardiovascular magnetic resonance (CMR) is widespread in clinical practice. The increased need to evaluate of subtle myocardial changes, coronary artery anatomy, and hemodynamic assessment has prompted the development of novel CMR techniques including T1 and T2 mapping, non-contrast angiography and four dimensional (4D) flow. T1 mapping is suitable for diagnosing pathologies affecting extracellular volume such as myocarditis, diffuse myocardial fibrosis and amyloidosis, and is a promising diagnostic tool for patients with iron overload and Fabry disease. T2 mapping is useful in depicting acute myocardial edema and estimating the amount of salvageable myocardium following an ischemic event. Novel angiography techniques, such as the self-navigated whole-heart or the quiescent-interval single-shot sequence, enable the visualization of the great vessels and coronary artery anatomy without the use of contrast material. The 4D flow technique overcomes the limitations of standard phase-contrast imaging and allows for the assessment of cardiovascular hemodynamics in the great arteries and flow patterns in the cardiac chambers. In conclusion, the future of CMR is heading toward a more reliable quantitative assessment of the myocardium, an improved non-contrast visualization of the coronary artery anatomy, and a more accurate evaluation of the cardiac hemodynamics.

Key words: Cardiac magnetic resonance; T1 mapping; Magnetic resonance angiography; T2 mapping; Four dimensional flow

Core tip: The increased need for the evaluation of subtle myocardial changes, coronary artery anatomy, and hemodynamic assessment has prompted the development of novel cardiovascular magnetic resonance (CMR) techniques including T1 and T2 mapping, non-contrast angiography and four dimensional flow. CMR is heading toward a more reliable quantitative assessment of the myocardium, an improved non-contrast visualization of the coronary artery anatomy, and a more accurate evaluation of the cardiac hemodynamics.

De Cecco CN, Muscogiuri G, Varga-Szemes A, Schoepf UJ. Cutting edge clinical applications in cardiovascular magnetic resonance. *World J Radiol* 2017; 9(1): 1-4 Available from: URL: http://www.wjgnet.com/1949-8470/full/v9/i1/1.htm DOI: http://dx.doi.org/10.4329/wjr.v9.i1.1

Cardiovascular magnetic resonance (CMR) has become a fundamental tool in the diagnostic and therapeutic pathways of several cardiac and vascular diseases. CMR allows for the fast and accurate assessment of cardiac anatomy and function, non-invasive tissue characterization, and blood flow quantification in a single examination. Standard pulse sequences such as T1-weighted and T2-weighted turbo spin echo (TSE) and late gadolinium enhancement (LGE) techniques are widely utilized for myocardial tissue characterization in clinical practice. T1 TSE sequences can depict fatty replacement in arrhythmogenic right ventricular cardiomyopathy, whereas T2-weighted imaging is essential for the evaluation of acute myocardial damage. LGE is important for the assessment of replacement fibrosis and pathologies characterized by myocardial interstitial space expansion.

Although the above techniques have been accepted for clinical application, the use of these sequences for myocardial tissue characterization has a number of limitations. For example, the myocardial signal intensity in T2-weighted images can be influenced by the proximity of the surface coils[1]. Qualitative evaluation of LGE images is operator-dependent and quantitative assessment is strongly influenced by the designated signal intensity threshold[2]. The value of the LGE technique may also be limited in cases with diffuse myocardial fibrosis[3]. Furthermore, it is important to note that LGE requires the administration of contrast agent and is, therefore, not suitable for patients with severe kidney dysfunction.

In order to overcome the aforementioned limitations, CMR sequences including T1 and T2 mapping have recently been developed.

T1 mapping was first introduced to detect diffuse myocardial fibrosis; however, this approach would also be beneficial in patients with congenital or acquired cardiac pathologies characterized by changes in myocardial extracellular space. In general, T1 mapping can be performed before and after contrast administration. By combining native and post-contrast T1 measurements, the myocardial partition coefficient can be derived, which allows for the calculation of the extracellular volume (ECV) after accounting for the patient's hematocrit (Figure 1)[4]. Because native T1 correlates with ECV, this technique may allow for tissue characterization in patients with kidney dysfunction, presenting a distinct advantage over LGE imaging techniques. The variation in the range of normal native T1 values stems from the use of different T1 mapping pulse sequences (inversion recovery *vs* saturation recovery), pulse sequence schemes, magnetic field strengths, *etc*[5]. Despite this variation, native T1 mapping has the potential to play a major role in the

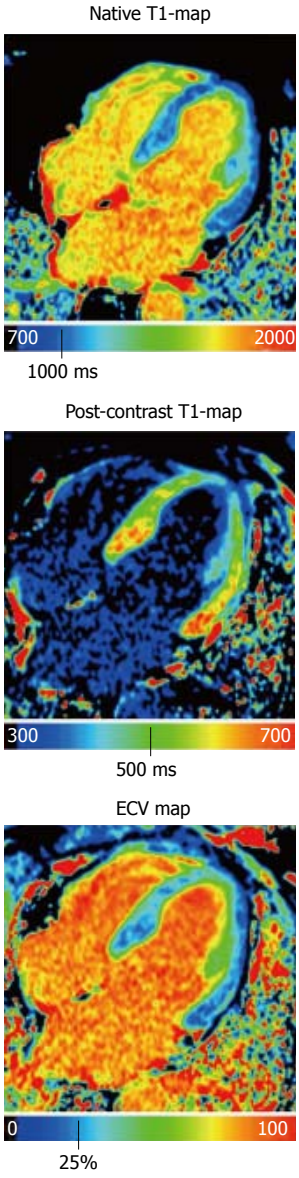

Figure 1 Native T1-map, post-contrast T1-map, and extracellular volume map of the myocardium in a healthy subject. ECV: Extracellular volume.

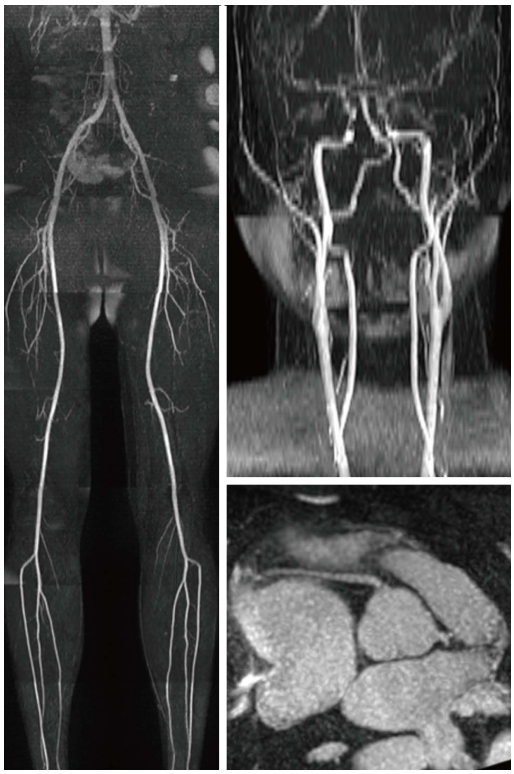

Figure 2 Visualization of the lower extremity, carotid and coronary arteries using quiescent-interval single-shot magnetic resonance angiography.

diagnosis of a variety of cardiac cases. Sado *et al*[6] showed that T1 mapping improves the detection of mild iron overload. Fontana *et al*[7] and Banypersad *et al*[8] showed that native T1 values are significantly higher in patients with cardiac amyloidosis compared to healthy controls and changes in native T1 and ECV can be considered prognostic biomarkers. Additionally, native T1 mapping may be essential in the differential diagnosis of Fabry disease as well as other cardiac diseases characterized by a hypertrophic phenotype[9].

T2 mapping is based on the collection of different T2-weighted images to sample the T2 decay. T2 mapping is useful for the evaluation of cardiac pathologies characterized by acute myocardial inflammation such as acute myocardial infarction, myocarditis, heart transplant rejection and Takotsubo cardiomyopathy[10].

Over the past few years, magnetic resonance angiography (MRA) has been surpassed by CT angiography in the clinical arena, mostly due to its faster acquisition time and the concerns related to gadolinium administration-induced nephrogenic systemic sclerosis (NSF). However, recent MR pulse sequence developments show substantial improvement in several aspects. For example, self-navigated whole-heart MRA provides a 3D volume involving the entire heart and the great vessels with an acquisition time of less than 7 min. In addition, it depends less on patient cooperation and can be performed in a free-breathing fashion in a predictable time frame with 100% image acquisition efficiency[11]. Quiescent-interval single-shot (QISS) MRA (Figure 2), another novel development, is a robust MRA technique available for both 1.5T and 3T acquisitions. QISS MRA has shown high diagnostic accuracy for the detection of significant arterial stenosis in the lower extremities compared to contrast-enhanced MRA and invasive catheter angiography[12,13]. QISS MRA has also shown promising results for coronary artery imaging[14].

The hemodynamic evaluation of blood flow in the great arteries and blood flow patterns in the cardiac chambers also play an important role in patient prognosis, particularly in congenital heart disease assessment. Four dimensional (4D) flow is a promising new technique that proves superior to standard phase-contrast imaging by providing additional information regarding the flow dynamics in the great arteries and flow pathways in both cardiac chambers and great vessels[15]. This added information about flow pathways in cardiac chambers and great vessels has the potential to aid in identifying left ventricular dysfunction in patients with dilated cardiomyopathy[16]. In addition, 4D flow allows for wall shear stress evaluation, which helps to better understand the pathologies involving the great vessels[17].

Considering the variety of new pulse sequences and their potential clinical applications, what is the future of CMR?

T1 and T2 mapping is expected to play a crucial role in depicting subtle myocardial changes. Both techniques may help to eliminate subjectivity in image analysis. The identification of disease-specific T1 and T2 normal ranges would be a great achievement for the accurate quantification of ECV expansion and detection of myocardial involvement. Novel MRA pulse sequences have the potential to broaden the range of clinical indications, providing a valid alternative to CT angiography. Finally, the 4D flow technique may advance understanding of the pathophysiology of different vascular diseases and the hemodynamic impact of flow abnormalities, as well as help with preoperative planning. In addition, a combined T1 mapping and 4D flow approach may provide a better understanding of the relationship between hemodynamics and changes in myocardial tissue[18].

In conclusion, CMR is heading toward a more reliable quantitative assessment of the myocardium, an improved non-contrast visualization of the coronary artery anatomy, and a more accurate evaluation of cardiac hemodynamics.

REFERENCES

1 **Giri S**, Chung YC, Merchant A, Mihai G, Rajagopalan S, Raman SV, Simonetti OP. T2 quantification for improved detection of myocardial edema. *J Cardiovasc Magn Reson* 2009; **11**: 56 [PMID: 20042111 DOI: 10.1186/1532-429X-11-56]

2 **McAlindon E**, Pufulete M, Lawton C, Angelini GD, Bucciarelli-Ducci C. Quantification of infarct size and myocardium at risk: evaluation of different techniques and its implications. *Eur Heart J Cardiovasc Imaging* 2015; **16**: 738-746 [PMID: 25736308 DOI:

10.1093/ehjci/jev001]
3 **Mewton N**, Liu CY, Croisille P, Bluemke D, Lima JA. Assessment of myocardial fibrosis with cardiovascular magnetic resonance. *J Am Coll Cardiol* 2011; **57**: 891-903 [PMID: 21329834 DOI: 10.1016/j.jacc.2010.11.013]
4 **White SK**, Sado DM, Fontana M, Banypersad SM, Maestrini V, Flett AS, Piechnik SK, Robson MD, Hausenloy DJ, Sheikh AM, Hawkins PN, Moon JC. T1 mapping for myocardial extracellular volume measurement by CMR: bolus only versus primed infusion technique. *JACC Cardiovasc Imaging* 2013; **6**: 955-962 [PMID: 23582361 DOI: 10.1016/j.jcmg.2013.01.011]
5 **Dabir D**, Child N, Kalra A, Rogers T, Gebker R, Jabbour A, Plein S, Yu CY, Otton J, Kidambi A, McDiarmid A, Broadbent D, Higgins DM, Schnackenburg B, Foote L, Cummins C, Nagel E, Puntmann VO. Reference values for healthy human myocardium using a T1 mapping methodology: results from the International T1 Multicenter cardiovascular magnetic resonance study. *J Cardiovasc Magn Reson* 2014; **16**: 69 [PMID: 25384607 DOI: 10.1186/s12968-014-0069-x]
6 **Sado DM**, Maestrini V, Piechnik SK, Banypersad SM, White SK, Flett AS, Robson MD, Neubauer S, Ariti C, Arai A, Kellman P, Yamamura J, Schoennagel BP, Shah F, Davis B, Trompeter S, Walker M, Porter J, Moon JC. Noncontrast myocardial T1 mapping using cardiovascular magnetic resonance for iron overload. *J Magn Reson Imaging* 2015; **41**: 1505-1511 [PMID: 25104503 DOI: 10.1002/jmri.24727]
7 **Fontana M**, Banypersad SM, Treibel TA, Maestrini V, Sado DM, White SK, Pica S, Castelletti S, Piechnik SK, Robson MD, Gilbertson JA, Rowczenio D, Hutt DF, Lachmann HJ, Wechalekar AD, Whelan CJ, Gillmore JD, Hawkins PN, Moon JC. Native T1 mapping in transthyretin amyloidosis. *JACC Cardiovasc Imaging* 2014; **7**: 157-165 [PMID: 24412190 DOI: 10.1016/j.jcmg.2013.10.008]
8 **Banypersad SM**, Fontana M, Maestrini V, Sado DM, Captur G, Petrie A, Piechnik SK, Whelan CJ, Herrey AS, Gillmore JD, Lachmann HJ, Wechalekar AD, Hawkins PN, Moon JC. T1 mapping and survival in systemic light-chain amyloidosis. *Eur Heart J* 2015; **36**: 244-251 [PMID: 25411195 DOI: 10.1093/eurheartj/ehu444]
9 **Thompson RB**, Chow K, Khan A, Chan A, Shanks M, Paterson I, Oudit GY. T+ mapping with cardiovascular MRI is highly sensitive for Fabry disease independent of hypertrophy and sex. *Circ Cardiovasc Imaging* 2013; **6**: 637-645 [PMID: 23922004 DOI: 10.1161/CIRCIMAGING.113.000482]
10 **Ferreira VM**, Piechnik SK, Robson MD, Neubauer S, Karamitsos TD. Myocardial tissue characterization by magnetic resonance imaging: novel applications of T1 and T2 mapping. *J Thorac Imaging* 2014; **29**: 147-154 [PMID: 24576837 DOI: 10.1097/RTI.0000000000000077]
11 **Piccini D**, Monney P, Sierro C, Coppo S, Bonanno G, van Heeswijk RB, Chaptinel J, Vincenti G, de Blois J, Koestner SC, Rutz T, Littmann A, Zenge MO, Schwitter J, Stuber M. Respiratory self-navigated postcontrast whole-heart coronary MR angiography: initial experience in patients. *Radiology* 2014; **270**: 378-386 [PMID: 24471387 DOI: 10.1148/radiol.13132045]
12 **Hodnett PA**, Koktzoglou I, Davarpanah AH, Scanlon TG, Collins JD, Sheehan JJ, Dunkle EE, Gupta N, Carr JC, Edelman RR. Evaluation of peripheral arterial disease with nonenhanced quiescent-interval single-shot MR angiography. *Radiology* 2011; **260**: 282-293 [PMID: 21502384 DOI: 10.1148/radiol.11101336]
13 **Hodnett PA**, Ward EV, Davarpanah AH, Scanlon TG, Collins JD, Glielmi CB, Bi X, Koktzoglou I, Gupta N, Carr JC, Edelman RR. Peripheral arterial disease in a symptomatic diabetic population: prospective comparison of rapid unenhanced MR angiography (MRA) with contrast-enhanced MRA. *AJR Am J Roentgenol* 2011; **197**: 1466-1473 [PMID: 22109304 DOI: 10.2214/AJR.10.6091]
14 **Edelman RR**, Giri S, Pursnani A, Botelho MP, Li W, Koktzoglou I. Breath-hold imaging of the coronary arteries using Quiescent-Interval Slice-Selective (QISS) magnetic resonance angiography: pilot study at 1.5 Tesla and 3 Tesla. *J Cardiovasc Magn Reson* 2015; **17**: 101 [PMID: 26597281 DOI: 10.1186/s12968-015-0205-2]
15 **Dyverfeldt P**, Bissell M, Barker AJ, Bolger AF, Carlhäll CJ, Ebbers T, Francios CJ, Frydrychowicz A, Geiger J, Giese D, Hope MD, Kilner PJ, Kozerke S, Myerson S, Neubauer S, Wieben O, Markl M. 4D flow cardiovascular magnetic resonance consensus statement. *J Cardiovasc Magn Reson* 2015; **17**: 72 [PMID: 26257141 DOI: 10.1186/s12968-015-0174-5]
16 **Eriksson J**, Bolger AF, Ebbers T, Carlhäll CJ. Four-dimensional blood flow-specific markers of LV dysfunction in dilated cardiomyopathy. *Eur Heart J Cardiovasc Imaging* 2013; **14**: 417-424 [PMID: 22879457 DOI: 10.1093/ehjci/jes159]
17 **Bürk J**, Blanke P, Stankovic Z, Barker A, Russe M, Geiger J, Frydrychowicz A, Langer M, Markl M. Evaluation of 3D blood flow patterns and wall shear stress in the normal and dilated thoracic aorta using flow-sensitive 4D CMR. *J Cardiovasc Magn Reson* 2012; **14**: 84 [PMID: 23237187 DOI: 10.1186/1532-429X-14-84]
18 **van Ooij P**, Allen BD, Contaldi C, Garcia J, Collins J, Carr J, Choudhury L, Bonow RO, Barker AJ, Markl M. 4D flow MRI and T1 -Mapping: Assessment of altered cardiac hemodynamics and extracellular volume fraction in hypertrophic cardiomyopathy. *J Magn Reson Imaging* 2016; **43**: 107-114 [PMID: 26227419 DOI: 10.1002/jmri.24962]

P- Reviewer: Mani V, Ni Y **S- Editor**: Ji FF **L- Editor**: A
E- Editor: Lu YJ

World Journal of Radiology

Submit a Manuscript: http://www.wjgnet.com/esps/
Help Desk: http://www.wjgnet.com/esps/helpdesk.aspx
DOI: 10.4329/wjr.v9.i1.5

World J Radiol 2017 January 28; 9(1): 5-9
ISSN 1949-8470 (online)

MINIREVIEWS

Functional magnetic resonance imaging and the brain: A brief review

Maggie SM Chow, Sharon L Wu, Sarah E Webb, Katie Gluskin, DT Yew

Maggie SM Chow, Sharon L Wu, DT Yew, School of Biomedical Science, School of Chinese Medicine, Chinese University of Hong Kong, Hong Kong, China

Sarah E Webb, Division of Life Science, the Hong Kong University of Science and Technology, Hong Kong, China

Katie Gluskin, Department of Neuroscience, St. Mary's College of Maryland, St Marys City, MD 20686, United States

Author contributions: Chow MSM, Wu SL, Webb SE and Gluskin K wrote the paper; Yew DT directed the research.

Conflict-of-interest statement: Authors declare no conflict of interest for this article.

Manuscript source: Invited manuscript

Correspondence to: Dr. Maggie SM Chow, School of Biomedical Science, School of Chinese Medicine, Chinese University of Hong Kong, Hong Kong, China. maggiesmchow@gmail.com
Telephone: +86-852-39434140

Received: June 16, 2016
Peer-review started: June 24, 2016
First decision: August 16, 2016
Revised: September 6, 2016
Accepted: October 22, 2016
Article in press: October 24, 2016
Published online: January 28, 2017

Abstract

Functional magnetic resonance imaging (fMRI) is employed in many behavior analysis studies, with blood oxygen level dependent- (BOLD-) contrast imaging being the main method used to generate images. The use of BOLD-contrast imaging in fMRI has been refined over the years, for example, the inclusion of a spin echo pulse and increased magnetic strength were shown to produce better recorded images. Taking careful precautions to control variables during measurement, comparisons between different specimen groups can be illustrated by fMRI imaging using both quantitative and qualitative methods. Differences have been observed in comparisons of active and resting, developing and aging, and defective and damaged brains in various studies. However, cognitive studies using fMRI still face a number of challenges in interpretation that can only be overcome by imaging large numbers of samples. Furthermore, fMRI studies of brain cancer, lesions and other brain pathologies of both humans and animals are still to be explored.

Key words: Functional magnetic resonance image; Blood oxygen level dependent imaging; Humans; Pig and rodent models; Aging; Drug effects; Brain lesions and disease

Core tip: We summarize the use of blood oxygen level dependent-contrast imaging in functional magnetic resonance imaging (fMRI) by introducing and comparing the various experimental and analysis methods used, as well as describing the results obtained, and the challenges that might occur in order to derive a hypothesis for further studies and exploration. In addition, an overview of fMRI following sensory stimulation in different specimen groups in both humans and animals is provided.

Chow MSM, Wu SL, Webb SE, Gluskin K, Yew DT. Functional magnetic resonance imaging and the brain: A brief review. *World J Radiol* 2017; 9(1): 5-9 Available from: URL: http://www.wjgnet.com/1949-8470/full/v9/i1/5.htm DOI: http://dx.doi.org/10.4329/wjr.v9.i1.5

INTRODUCTION

There have recently been a significant number of behavior response analysis studies that have made use of magnetic resonance imaging (MRI), and in particular functional magnetic resonance imaging (fMRI). The majority of these studies make use of blood oxygen level-dependent- (BOLD-) contrast imaging, which involves mapping particular regions of a functioning brain, from the changes in blood oxygen.

BOLD-contrast imaging fMRI has a good enough spatial resolution for the localization of activated brain areas and their delineation from neighbouring regions to be visualised. The voxel representing the area of activation is usually defined as covering a few million neurons[1]. In addition, the BOLD response lags 1 to 2 s behind the stimulus in order for the vascular system to respond, and in general it peaks at 5 s after the stimulus. A continuation of the same stimulus would downregulate the BOLD response[1-3]. A refractory period of just a few seconds is frequently inadequate for BOLD imaging after activation to fade (see below), depending on whether the mode of activation is motor, sensory or emotional.

To eliminate noise in the recording, the stimulus must be repeated several times. This process often takes a few minutes to complete, and the results can then be compared across different individuals or animals[1,4]. With regards to the latter, rodents, pigs and monkeys have all been employed in behavior response analysis studies with BOLD-contrast imaging fMRI[5-9]. This technique and thus the quality of images generated, has been improved by using both a spin echo pulse and increasing the magnetic strength[10].

One region of the brain that is popular for fMRI mapping due to it being relatively easy to generate a stimulus, is the sensory part of the brain, including the lateral geniculate bodies and the cortex[11]. Over the last ten years, our group has employed a number of different inputs of both sensory and motor activations for fMRI mapping, with some success. These include chewing, the opposition of the thumb (in humans) and passively flexing the elbow (in animals). These different types of activation trigger both the motor and the sensory systems, such as proprioception and movement[12,13]. However, only a limited number of clinical studies on head injuries, Alzheimer's disease and drug use have been documented using this method so far[4].

QUANTIFYING FMRI RESULTS

In the course of performing fMRI and comparing different specimen groups, it is often necessary to illustrate comparisons with quantitation. This can be achieved *via* a number of methods. For example, the different levels of oxygen usage are frequently illustrated with a pseudocolor scale in the images acquired. In the commonly used four-color scale, red indicates the highest level of oxygen uptake, yellow is an intermediate level of uptake, green indicates the normal level of oxygen, and blue indicates oxygen levels that are lower than normal (*i.e.*, down-regulation; Figure 1). Utilizing this type of color scale, the researcher can easily compare the volumes of the variously-colored regions either in a specific part of the brain or globally in the whole brain. Indeed, some well-funded research laboratories can afford to purchase software specifically designed to calculate the morphometry for this purpose. Another method used for quantitating fMRI images, which is perhaps more applicable to the smaller, less affluent groups involves manually counting squares on a simple grid. This is placed on successive slices of the fMRI image, after which volume data can be calculated. Though tedious, this method can yield results that are as accurate as those generated from expensive software packages.

In addition to quantitative analysis, qualitative evaluation is also important, for instance to determine the specific regions of the brain that are activated during a particular type of movement. Some of the areas that are activated might be nonspecific, in which case the investigator has to carefully consider each site of activation to determine if any logical deduction might be obtained. In this respect, at least six individuals, when available, should be used for every experiment in each group in order to obtain the n-numbers required to compare the data statistically. Indeed, in some of our previous studies, we aimed to recruit at least a dozen individuals per group. While this was not difficult to achieve with studies using animals, it was sometimes difficult to solicit this number of human volunteers or patients. In addition, we found that fMRI studies are particularly hard to evaluate when the experiments involve cognitive changes that might be affected by emotions. The results of psychometrical tests were variable in different individuals, especially in those with neurosis.

fMRI recordings require the subject (whether human or animal), to perform a particular action in order to trigger a dynamic uptake of oxygen into the brain. This is because fMRI recordings are based on the subsequent increase in oxygen demand from the brain tissue upon the execution of a certain stimulus, whether it is motor, sensory or emotional. One memorable case involved human subjects being asked to repeat a set words in the correct sequence, which elicited a notable increase of blood oxygen levels in the inferior frontal area (BA44) of the brain[14]. In this study, an uptake of oxygen was normally elicited after repeated and continuous stimulus, and the acquisition of the BOLD-contrast image was usually completed within several seconds after the stimulation ended (in this case after 6 to 18 s). The acquisition of subsequent BOLD-contrast images took > 1 s per slice, *e.g.,* 1.6 s[14]. The images acquired were then superimposed on the neuroanatomical image of the corresponding slices, which facilitated the localization of

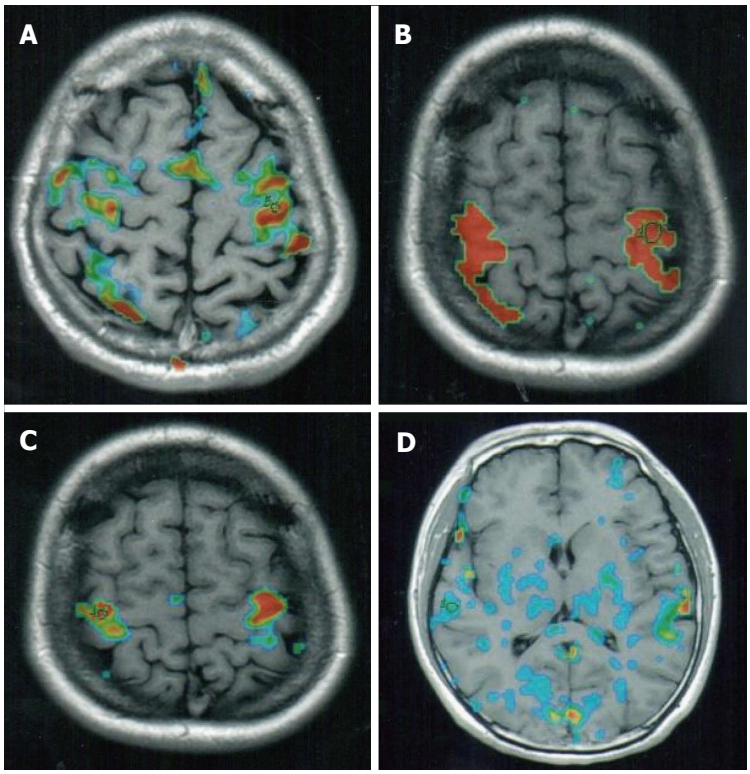

Figure 1 Functional magnetic resonance imaging image of different states. A: fMRI of a short term heroin addict at rest performing no activity and thus have no bodily stimulation. Note some areas still have high BOLD activity (red); B: fMRI of a short term heroin addict when performing motor and sensory activities. Note BOLD image in different regions showing high upregulation of BOLD (red), medium BOLD activity (yellow). While blue indicates downregulation of BOLD activities; C: fMRI of the same individual in (B) at rest after stimulation. There were still some high activity spots of BOLD after stimulation and at rest (red); D: fMRI of a long term (over 7 years) addict of heroin at rest. Many downregulated BOLD spots in the brain (blue). fMRI: Functional magnetic resonance imaging; BOLD: Blood oxygen level dependent.

the sites of recording[14].

FMRI HUMAN CASES AND DOWNREGULATION

In previous studies, we engaged human volunteers in active movements such as the opposition of the finger and thumb, flexion of the arm or mastication (*e.g.*, by chewing gum)[12,15]. In animals, such as pigs, rodents and monkeys, however, it is often difficult to capture fMRI images while they are freely and actively moving. Thus, passive movements tend to be performed instead. These include flexion and extension of the limbs and visual stimulation, as well as treatment with drugs.

In order to determine the effect of a specific behaviour on the amount of oxygen uptake in particular regions of the brain using fMRI, images acquired during movement and at rest must be compared. Indeed, valid data can be acquired by subtracting the results recorded at rest from those recorded during movement. Thus, subjects must be imaged as they perform a certain type of movement and then again when they are at rest. It would also be interesting to compare data from fMRI images acquired at different durations of rest after movement, as this might provide useful information regarding changes in the brain that occur during recovery after movement.

A typical example of a standard fMRI recording is depicted in Figure 1. Figure 1A indicates a recording that was acquired when the test subject was at rest. When we conducted this experiment, we were interested to find that in a number of individuals, some sporadic activity occurred in the cortex even at rest. In the recording of the individual shown in Figure 1, varying levels of activity were registered in the motor, sensory and visual areas of the brain, as well as in the midline of the cortex. Upon stimulation (achieved by thumb and finger opposition), clear and intensive reactions became apparent in the BOLD-contrast images, but these were limited to the motor and sensory areas alone (Figure 1B). Figure 1C depicts the corresponding fMRI image from the same individual following two minutes of stimulation and then one-minute of rest. It is still possible to recognise some residual increased brain activity in the post stimulation resting state. These figures demonstrate the importance of the timing used for the evaluation and comparison of data, as well as the use of the same individual for collecting corresponding sections in each series.

Another comparison method involves depicting of all the active sites of BOLD-contrast fMRI images in the whole brain both at rest and during stimulation. Both of these different methods of comparison are useful in their own way, with the comparison of corresponding slices providing a quantitation of comparison on specific sites, whereas the whole brain images provide a global picture of all the active sites.

In addition to recording the uptake of blood oxygen levels into the brain, the downregulation of blood oxygen has also recently been imaged by fMRI, in order to evaluate subjects with brain damage or brain defects. Figure 1D is an fMRI slice of the brain of long-term heroin addict. The large numbers of blue spots indicate regions of the brain where the blood oxygen levels are lower than normal (as described above, green indicates normal levels of oxygen). In the drug addict's brain, the blood oxygen was low (*i.e.*, downregulated) in the grey

matter, and also in the fibers, especially those in the corpus callosum (Figure 1D). These data confirm those acquired from ordinary MRI of addicts on abusive drugs, which also demonstrated degenerative sites[16], especially degenerative fibers or grey matter in the cortex, or in groups of nuclei in the cerebellum.

THE USE OF FMRI TO STUDY BRAIN DEVELOPMENT AND DISEASE

fMRI recordings are useful for evaluating the changes in the overall activity of specific brain regions, not only in adults, but also in developing and aging animals. For example, in one study, fMRI was conducted in the neonatal pig. At this stage of development the brain is relatively immature, and it was shown that stimulation of either sensory or motor activities in the body elicited a wide global and non-discrete response in the brain[7]. Several months later, stimulation of the same activities only produced induced BOLD responses in discrete and related areas of the brain. This example clearly shows that nonselective responses were elicited in the immature brain, whereas in the maturing or fully mature brain, the particular neuronal groups that fired were specific to the related functioning areas. The same type of global nonspecific firing observed in the fMRI of the immature brain can also be observed in some brain diseases such as schizophrenia and bipolar disorders. Follow-up cytochemical and histological studies conducted with the pig concluded that during the development and maturation of the brain, superfluous pathways were pruned significantly, and the number of inhibitory contacts that refine the specificity of each pathway of the brain increased. This study and others, demonstrated the usefulness of utilizing BOLD and fMRI for understanding psychiatric and neurological diseases, and they facilitated the collection of pathological specimens along the way at the same time. The use of fMRI imaging in conjunction with cytochemistry and/or classical pathohistological techniques has the potential to become a very powerful tool to help with the analysis of neurological diseases and mental disorders.

In addition to imaging the developing brain, fMRI can be applied to the aging brain. In a study employing humans of different ages (*i.e.*, young, middle-aged and old), BOLD-contrast imaging of fMRI was recorded in each group as they performed the same motor activities[12]. The results obtained were interesting and significant. More brain area activations were recorded in individuals in the "old" group (*i.e.*, around 70 years of age), when compared with individuals from the young and middle-aged groups as they conducted the same motor activity. It was concluded that the older brain is less efficient, and so larger areas are required to achieve a certain job. To substantiate this proposition, it was necessary to obtain a similar result in animals. As mentioned previously, specific active movements are a challenge to initiate in animals but passive movements are easier to control although the results obtained are more difficult to interpret. Therefore, in one a series of experiments we conducted, we used sensory stimulation in order to evaluate the aging hypothesis by applying a weight to the tail of rodents of different ages[17]. The results obtained with the rodents complimented those of the human studies in that the sensory stimulus triggered increased blood oxygen levels in larger areas of the brains of the older animals than in the young groups. It is therefore tempting to conclude that larger areas of the brain are recruited in the aging groups than in the young groups, to conduct the same functional activity. Perhaps this is due to brains being less efficient overall on aging. On the other hand, it is also possible that on aging it is normal for additional areas of the brain to be used to engage in activities. This would therefore illustrate the plasticity of the brain during aging rather than simply a reduction in the efficiency over time.

CHALLENGES AND FUTURE DIRECTIONS FOR FMRI STUDIES

Cognitive studies using fMRI are extremely important, but the results can be a challenge to interpret. The main difficulties lie in the psychometric nature of the individual to be recorded. For instance, some individuals are very anxious and when they are asked unrelated questions, this elicits responses in areas of the brain that are not normally engaged. Interpretation of data therefore depends on being able to collect a large enough number of samples to be able to exclude false positive results. fMRI imaging has largely been conducted with humans (including normal individuals, patients, addicts, and aged individuals), as well as in animal models of addiction and aging[18,19]. In the case of patients with various diseases, the way forward for fMRI and its potential are largely still under-explored. However, it might be very insightful to find out how areas of the brain areas react in patients with brain cancer, for example. It would also be interesting to explore any changes that might occur in focal pathological areas and in normal areas surrounding the pathology; as well as what changes take place in the brain as the disease progresses. These are just a few of the studies that might be conducted using BOLD-contrast fMRI.

REFERENCES

1 **Huettel SA**, Song AW, McCarthy G. Functional Magnetic resonance imaging. 2nd ed. Sunderland, Mass: Sinauer Associates, 2009: 1-501
2 **Dale AM**, Buckner RL. Selective averaging of rapidly presented individual trials using fMRI. *Hum Brain Mapp* 1997; **5**: 329-340 [PMID: 20408237 DOI: 10.1002/(SICI)1097-0193(1997)5: 5<329: : AID-HBM1>3.0.CO; 2-5]
3 **Kahn I**, Desai M, Knoblich U, Bernstein J, Henninger M, Graybiel AM, Boyden ES, Buckner RL, Moore CI. Characterization of the functional MRI response temporal linearity via optical control of

neocortical pyramidal neurons. *J Neurosci* 2011; **31**: 15086-15091 [PMID: 22016542 DOI: 10.1523/JNEUROSCI.0007-11.2011]

4 **Rombouts SA**, Bakhof L, Shelten P. Clinical applications of functional brain MRI. 1st edition. Oxford: Oxford University Press, 2008: 1-352

5 **Ogawa S**, Lee TM, Nayak AS, Glynn P. Oxygenation-sensitive contrast in magnetic resonance image of rodent brain at high magnetic fields. *Magn Reson Med* 1990; **14**: 68-78 [PMID: 2161986]

6 **Desai M**, Kahn I, Knoblich U, Bernstein J, Atallah H, Yang A, Kopell N, Buckner RL, Graybiel AM, Moore CI, Boyden ES. Mapping brain networks in awake mice using combined optical neural control and fMRI. *J Neurophysiol* 2011; **105**: 1393-1405 [PMID: 21160013 DOI: 10.1152/jn.00828.2010]

7 **Fang M**, Lorke DE, Li J, Gong X, Yew JC, Yew DT. Postnatal changes in functional activities of the pig's brain: a combined functional magnetic resonance imaging and immunohistochemical study. *Neurosignals* 2005; **14**: 222-233 [PMID: 16301837 DOI: 10.1159/000088638]

8 **Yu H**, Li Q, Wang D, Shi L, Lu G, Sun L, Wang L, Zhu W, Mak YT, Wong N, Wang Y, Pan F, Yew DT. Mapping the central effects of chronic ketamine administration in an adolescent primate model by functional magnetic resonance imaging (fMRI). *Neurotoxicology* 2012; **33**: 70-77 [PMID: 22178134 DOI: 10.1016/j.neuro.2011.11.001]

9 **Sun L**, Li Q, Li Q, Zhang Y, Liu D, Jiang H, Pan F, Yew DT. Chronic ketamine exposure induces permanent impairment of brain functions in adolescent cynomolgus monkeys. *Addict Biol* 2014; **19**: 185-194 [PMID: 23145560 DOI: 10.1111/adb.12004]

10 **Carr VA**, Rissman J, Wagner AD. Imaging the human medial temporal lobe with high-resolution fMRI. *Neuron* 2010; **65**: 298-308 [PMID: 20159444 DOI: 10.1016/j.neuron.2009.12.022]

11 **Kim SG**, Lee SP, Goodyear B, Silva AC, Moonen C, Bandettini PA. Medical Radiology: Diagnostic imaging, Functional MRI: Spatial resolution of BOLD and other fMRI techniques. Berlin: Springer, 2000: 453-463

12 **Fang M**, Li J, Lu G, Gong X, Yew DT. A fMRI study of age-related differential cortical patterns during cued motor movement. *Brain Topogr* 2005; **17**: 127-137 [PMID: 15974472]

13 **Fang M**, Li J, Rudd JA, Wai SM, Yew JC, Yew DT. fMRI mapping of cortical centers following visual stimulation in postnatal pigs of different ages. *Life Sci* 2006; **78**: 1197-1201 [PMID: 16182320 DOI: 10.1016/j.lfs.2005.06.030]

14 **Gore JC**. Principles and practice of functional MRI of the human brain. *J Clin Invest* 2003; **112**: 4-9 [PMID: 12840051 DOI: 10.1172/JCI19010]

15 **Jiang YL**, Tian W, Lu G, Rudd JA, Lai KF, Yeung LY, Wai MS, Li YY, Huang ML, Yew DT. Patterns of cortical activation following motor tasks and psychological-inducing movie cues in heroin users: an fMRI study. *Int J Psychiatry Med* 2014; **47**: 25-40 [PMID: 24956915]

16 **Wang C**, Zheng D, Xu J, Lam W, Yew DT. Brain damages in ketamine addicts as revealed by magnetic resonance imaging. *Front Neuroanat* 2013; **7**: 23 [PMID: 23882190 DOI: 10.3389/fnana.2013.00023]

17 **Zhang L**, Li Q, Wolff LT, Antonio GE, Yeung DK, Zhang A, Wu Y, Yew DT. Changes of brain activity in the aged SAMP mouse. *Biogerontology* 2007; **8**: 81-88 [PMID: 16955218 DOI: 10.1007/s10522-006-9035-9]

18 **Chan WM**, Xu J, Fan M, Jiang Y, Tsui TY, Wai MS, Lam WP, Yew DT. Downregulation in the human and mice cerebella after ketamine versus ketamine plus ethanol treatment. *Microsc Res Tech* 2012; **75**: 258-264 [PMID: 21809417 DOI: 10.1002/jemt.21052]

19 **Wai MS**, Rudd JA, Chan WY, Antonio GE, Yew DT. The effect of Ginkgo biloba on the cerebellum of aging SAMP mouse--a TUNEL, bcl-2, and fMRI study. *Microsc Res Tech* 2007; **70**: 671-676 [PMID: 17405152 DOI: 10.1002/jemt.20452]

P- Reviewer: Gao BL, Pan HC, Takahashi H **S- Editor**: Kong JX
L- Editor: A **E- Editor**: Lu YJ

World Journal of Radiology

Submit a Manuscript: http://www.wjgnet.com/esps/
Help Desk: http://www.wjgnet.com/esps/helpdesk.aspx
DOI: 10.4329/wjr.v9.i1.10

World J Radiol 2017 January 28; 9(1): 10-16
ISSN 1949-8470 (online)

ORIGINAL ARTICLE

Retrospective Study

Impact of contrast-enhanced ultrasound in patients with renal function impairment

Rossano Girometti, Tiziano Stocca, Elena Serena, Antonio Granata, Michele Bertolotto

Rossano Girometti, Institute of Diagnostic Radiology, Department of Medical and Biological Sciences, University of Udine, University Hospital "S. Maria della Misericordia", 33100 Udine, Italy

Tiziano Stocca, S.O.C. Radiologia, San Giovanni di Dio Hospital, 34170 Gorizia, Italy

Elena Serena, Michele Bertolotto, Department of Radiology, University of Trieste, Cattinara Hospital, Strada di Fiume, 34149 Trieste, Italy

Antonio Granata, UOC di Nefrologia-Dialisi, "San Giovanni di Dio" Hospital, 92100 Agrigento, Italy

Author contributions: Girometti R and Bertolotto M designed the study; Stocca T and Bertolotto M performed examinations; Stocca T, Serena E, Granata A and Bertolotto M analyzed images; Girometti R, Stocca T, Serena E, Granata A and Bertolotto M analyzed data; Girometti R and Bertolotto M wrote the paper.

Institutional review board statement: The study was reviewed and approved by the Ethical Committee of the Friuli Venezia Giulia, Italy.

Informed consent statement: By Italian regulations (Determinazione Ministeriale 20.03.2008, Delibera del 15.12.2011 del Garante per la Protezione dei Dati personali) informed consent acquisition is waived for retrospective studies.

Conflict-of-interest statement: Nothing to disclose.

Data sharing statement: No additional data are available.

Manuscript source: Invited manuscript

Correspondence to: Rossano Girometti, MD, Institute of Radiology, Department of Medical and Biological Sciences, University of Udine, University Hospital "S. Maria della Misericordia", via Colugna, 33100 Udine, Italy. rgirometti@sirm.org
Telephone: +39-0432-559266
Fax: +39-0432-559867

Received: June 11, 2016
Peer-review started: June 15, 2016
First decision: July 29, 2016
Revised: September 18, 2016
Accepted: November 1, 2016
Article in press: November 2, 2016
Published online: January 28, 2017

Abstract

AIM

To investigate the role of contrast enhanced ultrasound (CEUS) in evaluating patients with renal function impairment (RFI) showing: (1) acute renal failure (ARF) of suspicious vascular origin; or (2) suspicious renal lesions.

METHODS

We retrospectively evaluated patients addressed to CEUS over an eight years period to rule-out vascular causes of ARF (first group of 50 subjects) or assess previously found suspicious renal lesions (second group of 41 subjects with acute or chronic RFI). After preliminary grey-scale and color Doppler investigation, each kidney was investigated individually with CEUS, using 1.2-2.4 mL of a sulfur hexafluoride-filled microbubble contrast agent. Image analysis was performed in consensus by two readers who reviewed digital clips of CEUS. We calculated the detection rate of vascular abnormalities in the first group and performed descriptive statistics of imaging findings for the second group.

RESULTS

In the first group, CEUS detected renal infarction or

cortical ischemia in 18/50 patients (36%; 95%CI: 23.3-50.9) and 1/50 patients (2%; 95%CI: 0.1-12), respectively. The detection rate of infarction was significantly higher (P = 0.0002; McNemar test) compared to color Doppler ultrasonography (10%). No vascular causes of ARF were identified in the remaining 31/50 patients (62%). In the second group, CEUS detected 41 lesions on 39 patients, allowing differentiation between solid lesions (21/41; 51.2%) *vs* complex cysts (20/41; 48.8%), and properly addressing 15/39 patients to intervention when feasible based on clinical conditions (surgery and cryoablation in 13 and 2 cases, respectively). Cysts were categorized Bosniak Ⅱ, ⅡF, Ⅲ and Ⅳ in 8, 5, 4 and 3 cases, respectively. In the remaining two patients, CEUS found 1 pseudolesion and 1 subcapsular hematoma.

CONCLUSION

CEUS showed high detection rate of renal perfusion abnormalities in patients with ARF, influencing the management of patients with acute or chronic RFI and renal masses throughout their proper characterization.

Key words: Contrast-enhanced ultrasonography; Renal function impairment; Acute renal failure; Renal infarction; Renal lesions; Renal cysts; Bosniak classification

Core tip: Imaging in patients with renal function impairment (RFI) is challenging because of well-known limitations of conventional color Doppler ultrasound or risks related to the use of contrast media on computed tomography and magnetic resonance imaging. Contrast-enhanced ultrasound is a safer imaging tool in patients with RFI, showing 36% detection rate of renal infarction in patients with acute renal failure of suspicious vascular origin, and the capability of characterizing renal lesions in order to address patients to most proper treatment.

Girometti R, Stocca T, Serena E, Granata A, Bertolotto M. Impact of contrast-enhanced ultrasound in patients with renal function impairment. *World J Radiol* 2017; 9(1): 10-16 Available from: URL: http://www.wjgnet.com/1949-8470/full/v9/i1/10.htm DOI: http://dx.doi.org/10.4329/wjr.v9.i1.10

INTRODUCTION

Despite technical improvements, imaging of patients with renal function impairment (RFI) is challenging. Contrast-enhanced computed tomography (CT) and magnetic resonance imaging (MRI) provide panoramic representation of the kidneys, perirenal spaces, and vessels, leading to high diagnostic accuracy. However, iodinated contrast agents are potentially harmful in patients with RFI because of the risk of contrast-induced nephropathy (CIN)[1]. Although risk for nephrogenic systemic fibrosis (NSF) has been better defined over the last years, concerns still exist for the use of gadolinium chelates in patients with RFI, given uncertainty in pathogenic mechanisms and/or potential additional side effects related to gadolinium accumulation in the brain[1-4]. In practice, it is recommended to consider alternative imaging modalities in patients at risk with the use of iodinated or gadolinium contrast media[1].

Color-Doppler ultrasound (US) is the first imaging modality in patients with RFI. It is widely used to rule-out obstruction or investigate renal vessels and parenchymal abnormalities without the use of nephrotoxic agents[5]. In addition, US permits the detection of incidental, otherwise unknown renal lesions. However, there are well-known limitations of conventional Doppler modes in evaluating these patients, including difficult detection of perfusion abnormalities in globally hypoperfused kidneys, and unreliable characterization of renal masses other than simple cysts[5-8]. In particular, conventional Doppler modes do not allow differentiation between hypovascular tumors and complicated cysts[9,10], both of common occurrence in patients with RFI, nor can reliably assess the risk of malignancy of complex cystic masses.

Contrast-enhanced ultrasound (CEUS) has been advocated as the imaging modality of choice to evaluate patients with RFI, given the absence of nephrotoxicity and the ability of representing renal vascularization with excellent sensitivity and high spatial resolution[9,11]. According to the European federation of societies for ultrasound in medicine and biology (EFSUMB) guidelines, imaging with CEUS should be considered in every patient with RFI, when able to provide the clinically necessary information[1]. CEUS has the potential to compensate for limitations of conventional Doppler modes with a diagnostic performance comparable or superior to CT in the detection of perfusion abnormalities, lesion characterization (cystic *vs* solid), and categorization of cysts according to Bosniak criteria[10,12-14]. To our knowledge, however, evidence supporting the above indications results from reports on patients with normal renal function and experts opinion rather than specifically addressed studies, which currently lack.

The purpose of this study was to investigate the role of CEUS in a population of patients with RFI to assess the cause of renal function deterioration when perfusion abnormalities were clinically suspected or characterize renal lesions.

MATERIALS AND METHODS

Patient's population

Referring institutional review board approved this study and waived for informed consent acquisition due to the retrospective design, in accordance with regulations of our country. By performing a computer search, we identified all patients with RFI who underwent renal CEUS over an 8-years period (January 2004-August 2012) to assess the cause of renal function deterioration, or to attempt characterization of renal masses. Patients

Table 1 Sonographic equipment used in the study

Ultrasound equipment	Contrast-specific mode	No. of patients
MyLab-70 (EsaOte)	CnTI™ (contrast tuned imaging)	7
ATL HDI5000 (Philips)	PIHI™ (pulse inversion harmonic imaging)	15
Sequoia 512 (Acuson Siemens)	CPS™ (contrast pulse sequencing)	54
iU22 (Philips)	PIHI-PM™ (pulse inversion harmonic imaging – power modulation)	15

of the first group were investigated to rule-out a vascular cause for renal function deterioration. They were patients with risk factors for renal infarction manifesting a rapid decline of the estimated glomerular filtration rate (eGFR). In this group, conventional Doppler modes were used to investigate the renal arteries and parenchymal vessels, while CEUS was subsequently performed to rule-out infarcted areas not identified with conventional modes. Patients of the second group had renal masses identified on previous conventional US or unenhanced CT. All of them showed eGFR < 60 mL/min per 1.73 m^2 estimated from the serum creatinine values using the CKD-EPI equation[15]. Renal impairment was scored according to the grades of the National Kidney Foundation[16]. We assessed RFI according to the Kidney disease improving global outcomes (KDIGO) criteria for both acute renal failure (ARF)[17] and chronic renal failure (CRF)[18].

A total of 91 patients were enrolled (64 men, 27 women; age range 40-88 years; mean age 71.4 ± 11.02 years), showing renal impairment ranging from grade 3 to grade 5. Indications to CEUS were: (1) assessment of renal function deterioration in 50/91 patients; and (2) characterization of focal renal lesions in the remaining 41/91 patients.

CEUS technique

CEUS was performed using different ultrasound equipment and contrast-specific modes (Table 1). After preliminary grey-scale and color Doppler investigation, CEUS examination was set with low acoustic power to achieve minimum microbubble destruction (mechanical index between 0.06 and 0.2, depending on the equipment used). Each kidney was evaluated separately after *i.v.* injection of a 1.2-2.4 mL dose of a sulfur hexafluoride-filled microbubble contrast agent (SonoVue, BR1, Bracco, Milan, Italy). A 20-gauge cannula was used for contrast injection, followed by a 10 mL normal saline flush. Digital cine-clips were acquired to allow for post-procedure re-evaluation.

Image analysis

One radiologist with 18 years of experience in CEUS performed all the examinations. For the purpose of the study, he and a junior radiologist with five years of experience in this technique reviewed in consensus the images of conventional Doppler modes and the cine-clips of entire CEUS examinations, using a commercially available display workstation (OsiriX MD v.7.5, Pixmeo, Bernex, CH). Readers were blinded to histological diagnosis and/or follow-up results. No discrepancies were found between image interpretation at the time of examinations and during study review. Readers were asked to assess the presence of renal infarctions, characterize renal lesions as solid or cystic, and classify those with cystic appearance at CEUS according to the Bosniak criteria.

Readers assessed renal infarction on conventional Doppler modes in presence of parenchymal regions lacking color signal[19]. Concerning CEUS, we used the following diagnostic criteria: (1) infarction was diagnosed in presence of at least one well-defined, wedge-shaped non-enhancing area within an otherwise normal-appearing kidney[12]; (2) cortical ischemia was diagnosed in presence of enhancing interlobar and arcuate arteries with non-enhancing portions of the cortex[11]; and (3) a lesion was considered solid if more than half of the volume was represented by enhancing solid tissue, and cystic if composed predominantly of nonenhancing spaces[10,20]. Cystic lesions were graded according to the Bosniak criteria as previously described[13,14].

Data analysis

For the group of patients investigated to rule-out a vascular cause for renal function deterioration we calculated the detection rate of vascular abnormalities [(number of positive cases/total number of cases) × 100]. Analysis was performed on a per-patient basis by identifying at least one area of renal involvement. Significance of the difference between techniques in the detection rate of renal infarction was assessed with the McNemar test, using a reference alfa level of 0.01. Analysis was performed with a commercially available software (MedCalc v9.1, Mariakerke, Belgium).

For the group of patients with suspicious renal lesions we performed descriptive statistics of CEUS findings on a per-lesion basis.

RESULTS

Patients with acute RFI of suspicious vascular origin

Of fifty patients, 38 were males and 12 females (mean age: 71 ± 9 years, range 40-88 years). They presented with ARF either in previously well-functioning kidneys (31/50, 62%; 95%CI: 47.2-75.0), or complicating an already known CRF (19/50, 38%; 95%CI: 25.0-32.8). Causes of ARF were established based on clinical history and imaging follow-up in 44/50 cases (88%), renal biopsy in 3/50 cases (6.0%) and autopsy in the

Table 2 Overview of fifty patients with acute renal failure addressed to contrast-enhanced ultrasound to rule-out vascular causes

Findings on CEUS	Side of CEUS findings	Pre-existing renal function	Cause of acute renal failure	No. of patients with biopsy
Renal infarction (n = 18)	Unilateral (n = 13) Bilateral (n = 5)	Chronic RFI (n = 10) No previous history of RFI (n = 8)	Suspicious embolization (n = 2) Placement of aortic endoprothesis (n = 5) Aortic dissection (n = 2) Ischemia (n = 3) Drug-induced nephrotoxicity (n = 1) Undetermined (n = 5)	None
Acute cortical necrosis pattern (n = 1)	Bilateral (n = 1)	No previous history of RFI (n = 1)	Post-surgical, hypovolemic acute tubular necrosis (n = 1)	None
No vascular abnormalities (n = 31)	None	Chronic RFI (n = 21) No previous history of RFI (n = 10)	Atheroembolic disease (n = 10) Acute pyelonephritis (n = 4) Interstitial nephritis (n = 2) Acute papillary necrosis (n = 1) Antiblastic drug-induced (n = 1) Dehydration (n = 1) Undetermined (n = 12)	1 kidney biopsy, 3 skin biopsy 2 kidney biopsy

CEUS: Contrast enhanced ultrasound; RFI: Renal function impairment.

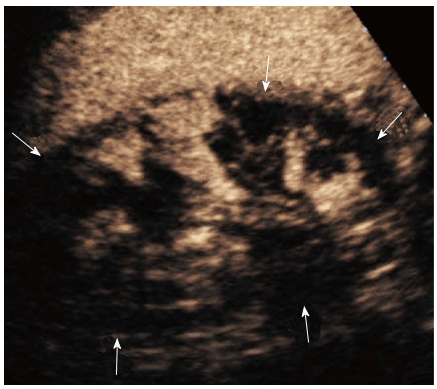

Figure 1 Patient with solitary kidney developing acute renal failure. Contrast enhanced ultrasound showed multiple renal infarctions (arrows) involving a large portion of the parenchyma.

remaining 3/50 cases (6.0%).

Renal infarction was found in 18/50 patients (36%; 95%CI: 23.3-50.9) using CEUS and 5/50 (10%; 95%CI: 3.7-22.6) using color Doppler US, corresponding to a significant difference in detection rate (P = 0.0002). In particular, CEUS found infarction in 13 additional subjects compared to color Doppler US (Figure 1). Moreover, CEUS identified acute cortical necrosis in one patient (2%; 95%CI: 0.1-12.0) presenting with non-specific hypoperfusion of the kidneys at color Doppler interrogation (Figure 2).

In the remaining 31/50 patients (62%; 95%CI: 47.2-75.0), there was no evidence of vascular abnormalities both on color Doppler US and CEUS. Final presumptive diagnosis was reached in 20/31 patients based on clinical and laboratory features, course of the disease and kidney biopsy in three subjects (two with interstitial nephritis and one with atheroembolic renal disease, respectively). Other three patients with atheroembolic renal disease had positive skin biopsy. In the remaining 12 patients, the cause of renal function deterioration remained undetermined. CEUS findings, pre-existing renal function and final diagnosis are reported in Table 2.

Patients with renal lesions

Of 41 patients included in this group, 26 were male and 15 female (mean age: 70 ± 14 years, range 41-90 years). CEUS showed a total of 41 lesions in 39 patients.

Twenty-one/41 lesions were solid in nature (51.2%; 95%CI: 35.4-66.8), whereas 20/41 lesions were assessed as complex cysts (48.8%; 95%CI: 33.2-64.6). Twelve out of 21 solid lesions were removed surgically, with final diagnosis of renal cancer, including 11 clear cell carcinomas (Figure 3) and 1 urothelial carcinoma. The remaining lesions included one oncocytoma diagnosed on autopsy, 7 indeterminate lesions addressed to imaging follow-up because of patients' age and comorbidities contraindicating surgery, and one inoperable lesion addressed to angiographic embolization because of acute intratumoral hemorrhage.

Cysts were classified according to Bosniak categories Ⅱ, ⅡF, Ⅲ and Ⅳ in 8, 5, 4 and 3 cases, respectively. All category ⅡF lesions, 1/4 category Ⅲ and 1/3 category Ⅳ cysts remained stable over a 3-years imaging follow-up (Figure 4). Two category Ⅲ cysts were a papillary and a clear cell renal cell carcinoma (RCC) on biopsy performed before percutaneous cryoablation. One category Ⅳ lesion was a clear cell RCC at nephrectomy (Figure 5). The remaining two patients (one with category Ⅲ, one with category Ⅳ cysts) were not operated because of clinically relevant comorbidities. Lesions increased in size and complexity over time and were considered presumably malignant. The remaining two patients with suspicious renal tumor on conventional US had a pseudotumour

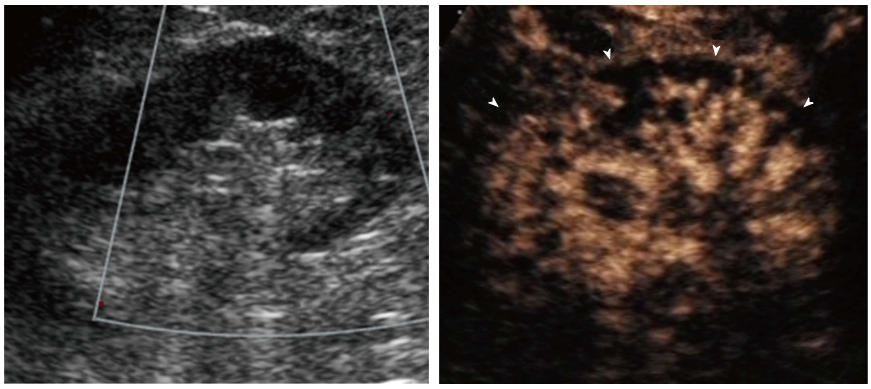

Figure 2 Patient with grade III chronic renal failure developing acute renal failure after Endovascular aortic repair. A: Color Doppler ultrasound showed avascular kidney; B: Contrast enhanced ultrasound showed enhancing hilar vessels and lack of enhancement of large portions of the cortex (arrowheads) consistent with acute cortical necrosis. The contralateral kidney was normal (not shown).

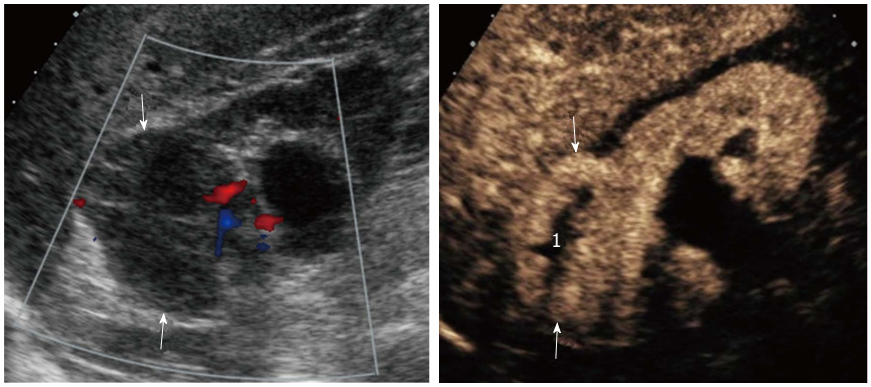

Figure 3 Patient with grade III chronic renal failure. A: Color Doppler ultrasound showed markedly reduced renal parenchyma perfusion and a hypoechoic lesion without obvious vascularity (arrows); B: Contrast enhanced ultrasound showed a solid enhancing mass (arrows) with avascular central portion (1). A clear cell RCC with necrotic central areas was found at surgery. RCC: Renal cell carcinoma.

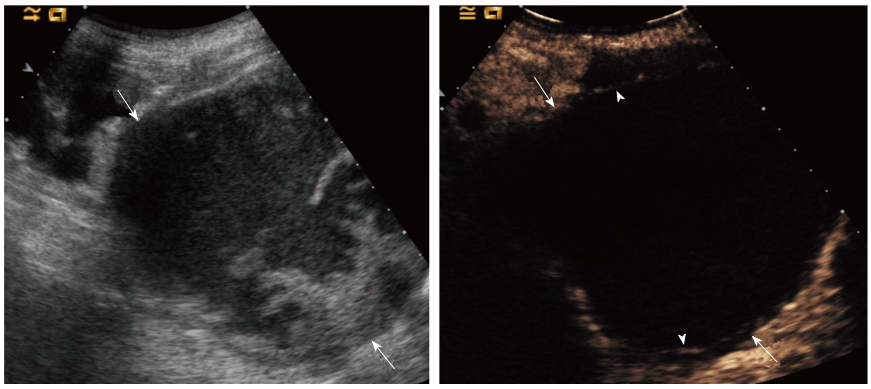

Figure 4 Patient with grade IV chronic renal failure. A: Grey-scale ultrasound showed a complex renal lesion (arrows). Contrast enhanced ultrasound showed no intralesional enhancement, nor vegetations; B: Two thin septa were visible (arrowheads) with minimum enhancement (benign minimally complicated cysts, Bosniak category II).

and a subcapsular hematoma at CEUS, respectively.

DISCUSSION

Current EFSUMB guidelines recommend use of CEUS in patients with RFI[1]. Indeed, this technique can be performed during the same examination session of color Doppler US, thus acting as first-line and problem-solving imaging modality at the same time[9,11].

However, indication to CEUS in this scenario is based more on theoretical considerations and experts opinion than on results of validation studies. Indeed, the ability of CEUS to identify renal infarction and to characterize complex cystic masses, pseudolesions, and hypovascular lesions has been mostly demonstrated in patients with well-functioning kidneys[10,12,13,21]. To our knowledge, no specific studies focused on patients with renal failure. Moreover, there is lack of evidence on whether information obtained with CEUS in patients with RFI has a clinical impact for patient management.

Our results on a consecutive series of patients with renal failure investigated with CEUS show that this technique is effective in identifying renal infarction and characterizing renal masses. When a vascular cause for the deterioration of the renal function was suspected, CEUS either confirmed the diagnosis or, when negative, prompted further clinical workup and eventually identification of other causes of renal function deterioration. CEUS clearly outperformed US with color Doppler, with a significantly higher detection rate of renal infarction (36% *vs* 10%) (P = 0.0002). Moreover, CEUS was able to differentiate between renal infarctions and cortical ischemia, which showed no definite correspondence on color Doppler US. Therefore, CEUS proved to be effective as problem solving technique in these patients, with the advantage of avoiding radiation

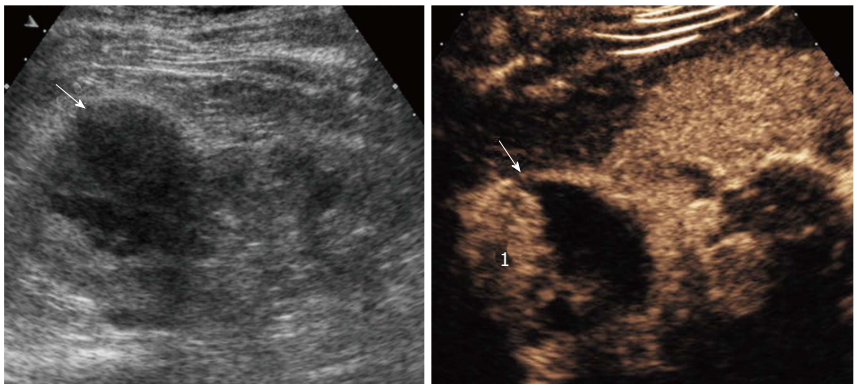

Figure 5 Patient with grade III chronic renal failure that one category IV lesion was a clear cell renal cell carcinoma at nephrectomy. A: Grey-scale ultrasound showed a complex renal lesion (arrow); B: Contrast enhanced ultrasound showed thickened wall with a vegetation (1) consistent for a presumably malignant, Bosniak category IV lesion. A clear cell renal cell carcinoma was found at surgery.

exposure or the use of nephrotoxic contrast agents. When renal lesions were identified in patients with renal failure, CEUS was able to discriminate between solid and cystic ones, as well as to categorize cysts according to the Bosniak criteria. Characterizing lesions with indeterminate appearance on conventional US modes as a presumably benign cysts prevented unnecessary operations in patients with renal failure (usually poor surgical candidates with high risk of complications), and further deterioration of the renal function.

Though cost-effectiveness analysis was beyond the purpose of this study, one can reasonably assume that evaluating the above patients with CEUS would led to prompt diagnosis and treatment while minimizing patients' risk and costs compared to conventional diagnostic strategy combining US and CT/MRI (including related complications). One might argue that the use of CEUS is often limited to experienced centers, and no randomized controlled trials support the above statements. However, the experience acquired in reference centres and guidelines recommendations (*e.g.*, EFSUMB ones) are now promoting an ever-increasing and widespread use of CEUS, as exemplified by extended indications to paediatric population[1]. We also believe that our study results might contribute as a reference for the planning of future studies designed to obtain high-level evidence in large populations with normal or impaired renal function. Potential effectiveness of CEUS diagnosis is further emphasized by the fact that this technique can be performed at patients' bedside, which is of special advantage for critically ill ones.

This study has several limitations. The most important one is that the gold standard investigation has not been obtained for the majority of patients with renal function deterioration. Because of the concern for further deterioration of renal function, no additional imaging modalities were performed when the results of CEUS and clinical features were found sufficient for patient's work-up. Only a limited number of patients with suspicious perfusion abnormalities had kidney biopsy (3/50 patients). As a consequence, causative diagnosis for renal function deterioration remained indeterminate in 5 patients with CEUS findings suggestive for renal infarction and 12 patients without CEUS evidence of vascular abnormalities. Gold standard investigation was not available also for 25/41 renal masses (8/21 solid lesions and 17/20 cysts), whereas 12 patients with presumably malignant renal lesions (7 solid indeterminate lesions, 1 inoperable solid lesion and 4 Bosniak Ⅲ-Ⅳ cysts) were not operated because the surgical risk was considered excessive due to comorbidities. However, all operated or ablated lesions (n = 15) were found to have cancer at histological examination, thus emphasizing the effectiveness of CEUS in guiding most proper treatment.

Another major limitation of the present study is its retrospective design. This might have introduced a case-selection bias, because some cases may have not been recorded for inclusion. Additionally, a relatively small number of lesions have been evaluated, reflecting the fact that CEUS has been performed as a problem solving technique to assess very specific diagnostic questions.

Finally, in our series CEUS failed to detect perfusion abnormalities in patients with atheroembolic renal disease. We can only speculate on the anatomic basis for this finding: atheroembolic renal disease consists in patchy embolization of very small arteries (interlobular and afferent arterioles) by cholesterol crystals resulting in cortical ischemic areas which are likely too small to be detected with imaging methods.

In conclusion, our study shows that CEUS has a significant role as a problem-solving technique for detection of perfusion abnormalities and characterization of renal lesions in patients with renal failure. CEUS can be performed in emergency at the bedside. In our series, it was helpful in stratifying treatment decisions, as shown by the fact that all patients with suspicious renal cancer in whom surgery was not contraindicated were operated properly.

ACKNOWLEDGMENTS

The authors thank Dr. Iliana Bednarova from the Institute of Radiology, University of Udine, for her help in revising English language.

COMMENTS

Background

Imaging in patients with acute or chronic renal function impairment (RFI) is challenging because of nephrotoxicity or the risk for nephrogenic systemic fibrosis (NSF) related to the use of computed tomography (CT) and magnetic

resonance imaging contrast agents, respectively. Contrast-enhanced ultrasound (CEUS) is gaining widespread acceptance as the imaging modality of choice to evaluate patients with RFI, given the absence nephrotoxicity and the ability of representing renal vascularization with excellent sensitivity and high spatial resolution. However, the consensus on its use in this setting is related more to experts' opinion and clinical practice than specifically addressed studies. Hence, evidence on this topic still lacks as a basis to support clinical practice and future trials.

Research frontiers

CEUS has a pivotal role in assessing patients with RFI. However, despite the use of CEUS in this scenario, there is paucity of scientific evidence supporting it. The results of the study show that CEUS has a significant impact in managing patients with RFI and might contribute to strengthen the recommendation to use it as the imaging method of choice in this setting.

Innovations and breakthroughs

The authors provided an evidence-based background for supporting the use of CEUS in patients with RFI. CEUS is safer than contrast-enhanced computed tomography and/or magnetic resonance imaging in evaluating patients with RFI. This technique can be performed on patients' bedside, thus allowing prompt diagnosis and management.

Applications

Their study shows that CEUS is a problem-solving technique in detecting perfusion abnormalities and characterizing renal lesions in patients with renal failure.

Terminology

CEUS: An ultrasound technique using microbubble contrast agents.

Peer-review

This is a well-written paper.

REFERENCES

1 **Piscaglia F**, Nolsøe C, Dietrich CF, Cosgrove DO, Gilja OH, Bachmann Nielsen M, Albrecht T, Barozzi L, Bertolotto M, Catalano O, Claudon M, Clevert DA, Correas JM, D'Onofrio M, Drudi FM, Eyding J, Giovannini M, Hocke M, Ignee A, Jung EM, Klauser AS, Lassau N, Leen E, Mathis G, Saftoiu A, Seidel G, Sidhu PS, ter Haar G, Timmerman D, Weskott HP. The EFSUMB Guidelines and Recommendations on the Clinical Practice of Contrast Enhanced Ultrasound (CEUS): update 2011 on non-hepatic applications. *Ultraschall Med* 2012; **33**: 33-59 [PMID: 21874631 DOI: 10.1055/s-0031-1281676]

2 **Thomsen HS**. Nephrogenic systemic fibrosis: A serious late adverse reaction to gadodiamide. *Eur Radiol* 2006; **16**: 2619-2621 [PMID: 17061066 DOI: 10.1007/s00330-006-0495-8]

3 **Thomsen HS**, Morcos SK, Almén T, Bellin MF, Bertolotto M, Bongartz G, Clement O, Leander P, Heinz-Peer G, Reimer P, Stacul F, van der Molen A, Webb JA. Nephrogenic systemic fibrosis and gadolinium-based contrast media: updated ESUR Contrast Medium Safety Committee guidelines. *Eur Radiol* 2013; **23**: 307-318 [PMID: 22865271 DOI: 10.1007/s00330-012-2597-9]

4 **Stojanov D**, Aracki-Trenkic A, Benedeto-Stojanov D. Gadolinium deposition within the dentate nucleus and globus pallidus after repeated administrations of gadolinium-based contrast agents-current status. *Neuroradiology* 2016; **58**: 433-441 [PMID: 26873830 DOI: 10.1007/s00234-016-1658-1]

5 **Pozzi Mucelli R**, Bertolotto M, Quaia E. Imaging techniques in acute renal failure. *Contrib Nephrol* 2001; **132**: 76-91 [PMID: 11395914]

6 **Kim SH**, Cho JY, Kim SY, Moon KC, Kwak C, Kim HH. Ultrasound Evaluation of Renal Masses: Gray-scale, Doppler, and More. *Ultrasound Clinics* 2013; **8**: 565-579 [DOI: 10.1016/j.cult.2013.07.002]

7 **Cantisani V**, Bertolotto M, Weskott HP, Romanini L, Grazhdani H, Passamonti M, Drudi FM, Malpassini F, Isidori A, Meloni FM, Calliada F, D'Ambrosio F. Growing indications for CEUS: The kidney, testis, lymph nodes, thyroid, prostate, and small bowel. *Eur J Radiol* 2015; **84**: 1675-1684 [PMID: 26014102 DOI: 10.1016/j.ejrad.2015.05.008]

8 **Pozzi Mucelli R**, Bertolotto M. Imaging techniques in acute renal failure. *Kidney Int* 1998; **66**: S102-S105

9 **Bertolotto M**, Derchi LE, Cicero C, Iannelli M. Renal Masses as Characterized by Ultrasound Contrast. *Ultrasound Clin* 2013; **8**: 581-592 [DOI: 10.1016/j.cult.2013.07.003]

10 **Bertolotto M**, Cicero C, Perrone R, Degrassi F, Cacciato F, Cova MA. Renal Masses With Equivocal Enhancement at CT: Characterization With Contrast-Enhanced Ultrasound. *AJR Am J Roentgenol* 2015; **204**: W557-W565 [PMID: 25905962 DOI: 10.2214/AJR.14.13375]

11 **Granata A**, Zanoli L, Insalaco M, Valentino M, Pavlica P, Di Nicolò PP, Scuderi M, Fiorini F, Fatuzzo P, Bertolotto M. Contrast-enhanced ultrasound (CEUS) in nephrology: Has the time come for its widespread use? *Clin Exp Nephrol* 2015; **19**: 606-615 [PMID: 25351822 DOI: 10.1007/s10157-014-1040-8]

12 **Bertolotto M**, Martegani A, Aiani L, Zappetti R, Cernic S, Cova MA. Value of contrast-enhanced ultrasonography for detecting renal infarcts proven by contrast enhanced CT. A feasibility study. *Eur Radiol* 2008; **18**: 376-383 [PMID: 17851664 DOI: 10.1007/s00330-007-0747-2]

13 **Ascenti G**, Mazziotti S, Zimbaro G, Settineri N, Magno C, Melloni D, Caruso R, Scribano E. Complex cystic renal masses: characterization with contrast-enhanced US. *Radiology* 2007; **243**: 158-165 [PMID: 17392251 DOI: 10.1148/radiol.2431051924]

14 **Quaia E**, Bertolotto M, Cioffi V, Rossi A, Baratella E, Pizzolato R, Cov MA. Comparison of contrast-enhanced sonography with unenhanced sonography and contrast-enhanced CT in the diagnosis of malignancy in complex cystic renal masses. *AJR Am J Roentgenol* 2008; **191**: 1239-1249 [PMID: 18806171 DOI: 10.2214/AJR.07.3546]

15 **Levey AS**, Stevens LA, Schmid CH, Zhang YL, Castro AF, Feldman HI, Kusek JW, Eggers P, Van Lente F, Greene T, Coresh J. A new equation to estimate glomerular filtration rate. *Ann Intern Med* 2009; **150**: 604-612 [PMID: 19414839]

16 **Levey AS**, Eckardt KU, Tsukamoto Y, Levin A, Coresh J, Rossert J, De Zeeuw D, Hostetter TH, Lameire N, Eknoyan G. Definition and classification of chronic kidney disease: a position statement from Kidney Disease: Improving Global Outcomes (KDIGO). *Kidney Int* 2005; **67**: 2089-2100 [PMID: 15882252 DOI: 10.1111/j.1523-1755.2005.00365.x]

17 KDIGO Clinical Practice Guideline for Acute Kidney Injury. *Kidney International Supplements* 2012; **2**: 8-12 [DOI: 10.1038/kisup.2012.7]

18 **Levey AS**, Coresh J, Balk E, Kausz AT, Levin A, Steffes MW, Hogg RJ, Perrone RD, Lau J, Eknoyan G. National Kidney Foundation practice guidelines for chronic kidney disease: evaluation, classification, and stratification. *Ann Intern Med* 2003; **139**: 137-147 [PMID: 12859163 DOI: 10.7326/0003-4819-139-2-200307150-00013]

19 **Hélénon O**, el Rody F, Correas JM, Melki P, Chauveau D, Chrétien Y, Moreau JF. Color Doppler US of renovascular disease in native kidneys. *Radiographics* 1995; **15**: 833-854; discussion 854-865 [PMID: 7569132 DOI: 10.1148/radiographics.15.4.7569132]

20 **Tamai H**, Takiguchi Y, Oka M, Shingaki N, Enomoto S, Shiraki T, Furuta M, Inoue I, Iguchi M, Yanaoka K, Arii K, Shimizu Y, Nakata H, Shinka T, Sanke T, Ichinose M. Contrast-enhanced ultrasonography in the diagnosis of solid renal tumors. *J Ultrasound Med* 2005; **24**: 1635-1640 [PMID: 16301719]

21 **Mazziotti S**, Zimbaro F, Pandolfo A, Racchiusa S, Settineri N, Ascenti G. Usefulness of contrast-enhanced ultrasonography in the diagnosis of renal pseudotumors. *Abdom Imaging* 2010; **35**: 241-245 [PMID: 19194642 DOI: 10.1007/s00261-008-9499-y]

P- Reviewer: Abou El-Ghar M, Markic D, Salvi PF, Scarpioni R, Watanabe T **S- Editor**: Qiu S **L- Editor**: A **E- Editor**: Lu YJ

World Journal of Radiology

Submit a Manuscript: http://www.wjgnet.com/esps/
Help Desk: http://www.wjgnet.com/esps/helpdesk.aspx
DOI: 10.4329/wjr.v9.i1.17

World J Radiol 2017 January 28; 9(1): 17-26
ISSN 1949-8470 (online)

ORIGINAL ARTICLE

Prospective Study

Multimodality functional imaging using DW-MRI and ^{18}F-FDG-PET/CT during radiation therapy for human papillomavirus negative head and neck squamous cell carcinoma: Meixoeiro Hospital of Vigo Experience

David Aramburu Núñez, Antonio Lopez Medina, Moisés Mera Iglesias, Francisco Salvador Gomez, Abhay Dave, Vaios Hatzoglou, Ramesh Paudyal, Alfonso Calzado, Joseph O Deasy, Amita Shukla-Dave, Victor M Muñoz

David Aramburu Núñez, Antonio Lopez Medina, Francisco Salvador Gomez, Department of Medical Physics and Radiological Protection, Galaria - Meixoeiro, University Hospital Complex of Vigo, 36200 Vigo, Spain

David Aramburu Núñez, Abhay Dave, Ramesh Paudyal, Joseph O Deasy, Amita Shukla-Dave, Department of Medical Physics, Memorial Sloan-Kettering Cancer Center, New York, NY 10065, United States

David Aramburu Núñez, Alfonso Calzado, Department of Radiology, Complutense University, 28040 Madrid, Spain

Moisés Mera Iglesias, Department of Medical Physics, Oncoserv, Santiago de los Caballeros 51000, Dominican Republic

Vaios Hatzoglou, Amita Shukla-Dave, Department of Radiology, Memorial Sloan-Kettering Cancer Center, New York, NY 10065, United States

Victor M Muñoz, Department of Radiation Oncology, Galaria - Meixoeiro, University Hospital Complex of Vigo, 36200 Vigo, Spain

Author contributions: Aramburu Núñez D, Lopez Medina A and Shukla-Dave A designed the study, performed MRI research, analyzed the data and wrote the paper; Dave A and Paudyal R analyzed the data and reviewed the paper; Mera Iglesias M and Salvador Gomez F performed MRI research and provided software support; Muñoz VM enrolled patients, and performed clinical assessment as per standard of care; Hatzoglou V performed the radiologic assessment; Calzado A and Deasy JO provided support.

Supported by The National Health Institute of Spain: ISCIII Grant PI11/02035 and DTS14/00188; BIOCAPS project (FP7/REGPOT-2012-2013.1), No. 316265; MSKCC internal IMRAS grant; and in part through the NIH/NCI Cancer Center, No. P30 CA008748.

Institutional review board statement: Six patients were enrolled in the Meixoeiro Hospital of Vigo Research Protocol entitled "Radioterapia adaptativa y predicción de la respuesta tumoral basadas en estudios funcionales de RM y PET/CT en cáncer de cabeza y cuello" (ISCIII Grant PI1102035).

Informed consent statement: All patients gave informed consent for their participation in the study approved by the hospital, which was conducted in accordance with the Declaration of Helsinki.

Conflict-of-interest statement: All authors have no conflicts of interest with regard to this manuscript.

Data sharing statement: Upon formal request and with proper motivation, all original data in anonymized format is available from the corresponding author for local inspection, but cannot leave Meixoeiro Hospital of Vigo and Memorial Sloan Kettering Cancer Center.

Manuscript source: Invited manuscript

Correspondence to: Amita Shukla-Dave, PhD, Director Quantitative Imaging, Department of Medical Physics, Memorial Sloan-Kettering Cancer Center, 1275 York Avenue, New York, NY 10065, United States. davea@mskcc.org

Telephone: +1-212-6393184
Fax: +1-212-7173010

Received: August 17, 2016
Peer-review started: August 18, 2016
First decision: October 21, 2016
Revised: October 29, 2016
Accepted: November 21, 2016
Article in press: November 23, 2016
Published online: January 28, 2017

Abstract

AIM

To noninvasively investigate tumor cellularity measured using diffusion-weighted magnetic resonance imaging (DW-MRI) and glucose metabolism measured by ^{18}F-labeled fluorodeoxyglucose positron emission tomography/computed tomography (^{18}F-FDG-PET/CT) during radiation therapy (RT) for human papillomavirus negative (HPV-) head and neck squamous cell carcinoma (HNSCC).

METHODS

In this prospective study, 6 HPV- HNSCC patients underwent a total of 34 multimodality imaging examinations (DW-MRI at 1.5 T Philips MRI scanner [(n = 24) pre-, during- (2-3 wk), and post-treatment (Tx), and ^{18}F-FDG PET/CT pre- and post-Tx (n = 10)]. All patients received RT. Monoexponential modeling of the DW-MRI data yielded the imaging metric apparent diffusion coefficient (ADC) and the mean of standardized uptake value (SUV) was measured from ^{18}F-FDG PET uptake. All patients had a clinical follow-up as the standard of care and survival status was documented at 1 year.

RESULTS

There was a strong negative correlation between the mean of pretreatment ADC (ρ = -0.67, P = 0.01) and the pretreatment ^{18}F-FDG PET SUV. The percentage (%) change in delta (Δ) ADC for primary tumors and neck nodal metastases between pre- and Wk2-3 Tx were as follows: 75.4% and 61.6%, respectively, for the patient with no evidence of disease, 27.5% and 32.7%, respectively, for those patients who were alive with disease, and 26.9% and 7.31%, respectively, for those who were dead with disease.

CONCLUSION

These results are preliminary in nature and are indicative, and not definitive, trends rendered by the imaging metrics due to the small sample size of HPV- HNSCC patients in a Meixoeiro Hospital of Vigo Experience.

Key words: Diffusion-weighted magnetic resonance imaging; Human papillomavirus negative head and neck squamous cell carcinoma; ^{18}F-labeled fluorodeoxyglucose positron emission tomography/computed tomography

Core tip: In the modern era of adaptive radiotherapy, it is crucial to understand how different imaging techniques interact and complement each other for application in cancer care. The quantitative imaging metrics, apparent diffusion coefficient and standardized uptake value, play a significant role in understanding the efficacy of the radiotherapy treatment. Tumor cellularity and glucose metabolism were investigated before, during, and after radiotherapy in human papillomavirus negative head and neck squamous cell carcinoma patients using the diffusion-weighted magnetic resonance imaging and ^{18}F-labeled fluorodeoxyglucose positron emission tomography/computed tomography imaging techniques.

Aramburu Núñez D, Lopez Medina A, Mera Iglesias M, Salvador Gomez F, Dave A, Hatzoglou V, Paudyal R, Calzado A, Deasy JO, Shukla-Dave A, Muñoz VM. Multimodality functional imaging using DW-MRI and ^{18}F-FDG-PET/CT during radiation therapy for human papillomavirus negative head and neck squamous cell carcinoma: Meixoeiro Hospital of Vigo Experience. *World J Radiol* 2017; 9(1): 17-26 Available from: URL: http://www.wjgnet.com/1949-8470/full/v9/i1/17.htm DOI: http://dx.doi.org/10.4329/wjr.v9.i1.17

INTRODUCTION

The Spanish Cancer Registries reported that in 2014, 241284 new cases of cancer were diagnosed in Spain[1]. Out of these, 12696 were head and neck (HN) cancers in which approximately 90% were specifically squamous cell carcinomas (SCC)[2]. The main subgroup for the patients was oropharyngeal SCC wherein 52%-72% of the cases were caused by infection from the human papillomavirus (HPV)[3]. It has been previously reported that HPV negative (-) HNSCC patients have poor outcomes compared with HPV-positive (HPV+) cancers[4]. Thus, in an effort to perform biologically guided adaptive radiotherapy, it is critical to understand how different functional imaging techniques interact and potentially complement each other[5]. Multimodality imaging, such as diffusion-weighted magnetic resonance imaging (DW-MRI) and ^{18}F-labeled fluorodeoxyglucose positron emission tomography/computed tomography (^{18}F-FDG-PET/CT), can provide useful anatomical and functional quantitative imaging metrics.

DW-MRI provides a noninvasive measurement for the degree of random motion of water in tissue; the rate of this diffusion is quantified by a quantitative imaging metric, the apparent diffusion coefficient (ADC)[6]. The advantage of DW-MRI over traditional anatomical MRI is that it can reflect the tissue cellularity and the integrity of cell membranes[7]. A recent metaanalysis reported that ADC has an inverse correlation with tissue cell density[8]. Kim *et al*[9] have shown that a significant increase in ADC was observed within 1 wk of treatment in HNSCC patients who were complete responders (P < 0.01). The Vandecaveye

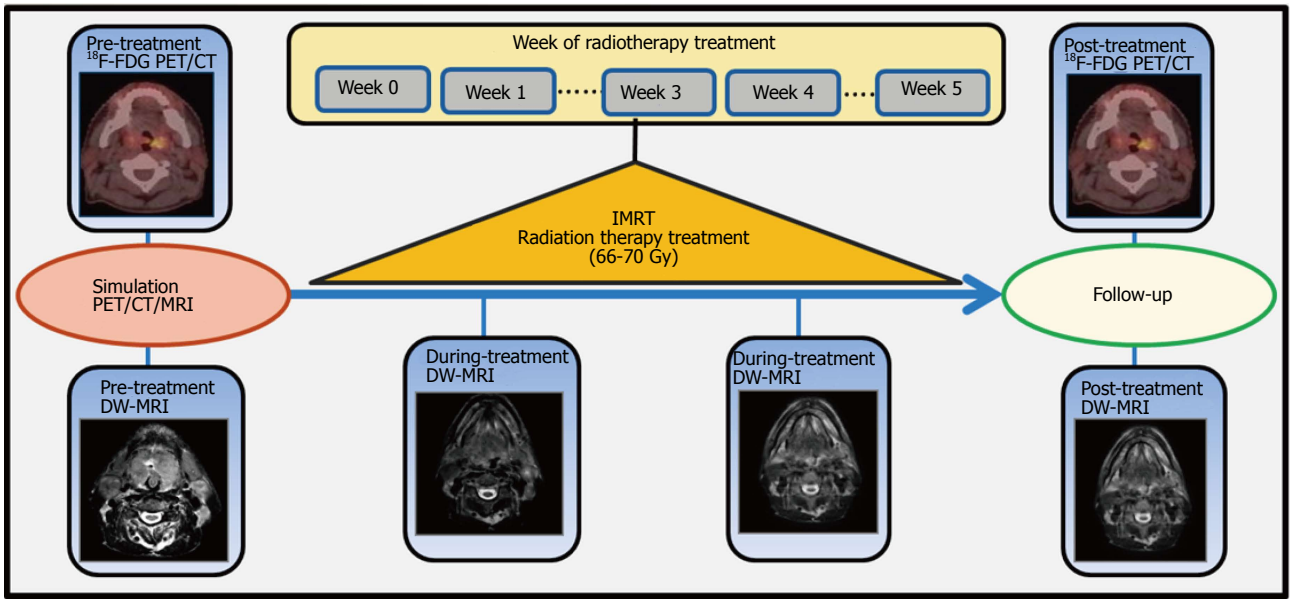

Figure 1 Workflow representing the study design performed in all the patients. ^{18}F-FDG: Fluorine-18 Fludeoxyglucose; PET/CT: Positron emission tomography/computed tomography; DW-MRI: Diffusion-weighted magnetic resonance imaging.

et al[10] study further established the utility of ADC in differentiating responding from non-responding HNSCC by providing a threshold (25% and 20% for primary tumors and lymph node metastases, respectively) for the percent relative (Δ) ADC change between pre-treatment (Tx) and 3 wk post-chemoradiotherapy (post-CRT).

Another quantitative imaging metric, standardized uptake value (SUV), obtained from ^{18}F-FDG PET is a measure of glucose metabolism. An abnormally elevated SUV can be observed in most primary and metastatic cancers including HNSCC[11]. The ^{18}F-FDG PET/CT has an established role in HNSCC management, including staging and monitoring CRT response[12,13]. The Schwartz *et al*[14] study showed that primary tumor SUV was a promising prognostic factor in HNSCC patients.

A better understanding of the association between ^{18}F-FDG PET/CT and DW-MRI derived quantitative imaging metrics is needed in order for them to become the building blocks for a biologically-guided adaptive radiotherapy. Recently there have been few reports showing correlations between these multimodality imaging techniques and their initial role in the prognosis of HNSCC patients[15]. However, there are limited studies initiated to explore the use of these techniques together in a treatment planning setting for radiation oncology[16]. Our study is the first experience in Spain with multimodality imaging in HPV-HNSCC patients for its use in biologically-guided adaptive radiotherapy. The purpose of the current study is to non-invasively investigate tumor cellularity measured using DW-MRI and glucose metabolism measured by ^{18}F-FDG-PET/CT during RT for HPV- HNSCC.

MATERIALS AND METHODS

Patients

This prospective study was conducted in accordance with the Declaration of Helsinki[17]. The study protocol was approved by the local ethics committee; informed consent was obtained from all patients. All patients eligible for this study had biopsy-proven newly diagnosed squamous cell carcinoma of the head and neck. Diagnostic biopsies were also performed to evaluate HPV status. Six HPV- HNSCC patients underwent a total of 34 multimodality imaging examinations [DW-MRI at 1.5 T Philips MRI scanner (n = 24) pre-, during (2-3 wk) and post-Tx, and ^{18}F-FDG PET/CT pre- and post-Tx (n = 10)] (Figure 1). All the patients were treated with intensity-modulated radiation therapy (IMRT), and the prescribed doses varied between 66 Gy and 70 Gy to the local planning target volume (PTV). Patient characteristics are given in Table 1.

All the patients had a clinical follow-up as the standard of care and survival status was documented into groups at 1 year. The four groups for patients were as follows: No evidence of disease (NED), alive with disease (AWD), dead of disease (DOD), and dead of other causes (DOC). Additionally, local-regional and distant metastases statuses were noted for all patients[18].

DWI-MRI

All MRI examinations were performed on a 1.5-Tesla Achieva scanner (Philips Healthcare, The Netherlands) with a Philips Sense Flex coil over the neck. For MRI, all patients were in the supine position with an immobilization system that was also used during the radiotherapy treatment delivery. A thermoplastic mask, head support, and flat table were used to minimize distortion and improve the registration process between the different imaging modalities. The head support and flat table were adapted to the MRI/safety requirements. The MRI protocol consisted of the standard anatomic MRI scans (T1-/T2-weighted images) and DW-MRI.

DW-MRI acquisition was performed using single-shot echo planar imaging (SS-EPI) with three b values (b =

Table 1 Characteristics of the patients involved in this study

Characteristics	Value
Demographics	
Mean age (yr)	65
Age range (yr)	52-79
Male/female	5/1
Location of primary tumor	
Oropharynx	6
Metastatic loco-regional nodes	11
Radiation therapy technique	IMRT
Dose (Gy)	66-70
Fractions	32
Outcome	
Alive with disease	3
Dead of disease	2
No evidence of disease	1

0, 600 and 1000 s/mm^2). Other parameters included repetition time (TR) = 5000 ms, echo time (TE) = 77-100 ms, number of excitations (NEX) = 2, field of view (FOV): 24 cm, and slice thickness = 6 mm. The total acquisition time for obtaining the DW-MRI data was approximately 5 min. The acquisition matrix of 120 × 97 was zero filled to 256 × 256 during image reconstruction.

^{18}F-FDG PET/CT

A whole-body PET/CT scan was performed from head to thigh, 60 min after intravenous administration of approximately 370 MBq (± 10%) of ^{18}F-FDG on a PET/CT Discovery scanner (GE Healthcare Bio-Sciences Corp.). The patient was placed in the supine position, with the same immobilization system as in the radiotherapy treatment delivery. Other parameters included a 70 cm axial FOV, a 218 × 218 matrix. Data was acquired in a 3-D mode. The pixel spacing was 5.47 mm with a slice thickness of 3.27 mm. The spatial resolution varied from 3.99 mm to 4.56 mm. PET images were corrected using the specific software of the equipment for attenuation, scatter, decay, dead time, random coincidences, and slice sensitivity.

Image analysis

All images were registered and analyzed using in-house software (Artfibio-tool)[19]. The registration for DW-MRI and ^{18}F-FDG PET/CT datasets was a two-step process: (1) Manual registration: performing a manual alignment (translation and/or rotation) of the images (DWMRI, CT-Scan, PET-CT) interactively on-screen; and (2) Automatic Rigid Registration: Once the images were approximately aligned, a more precise alignment (full rigid transformation) was performed based on an iterative process evaluated by statistical metrics (Viola and Wells mutual information[20]). Using Artfibio-tool, the signal intensity values were extracted from the whole tumor volumes[19].

DW-MRI: According to Stejskal and Tanner's[21] and considering the monoexponential approximation (7), the ADC value was calculated using equation 1:

$$ADC = [\log_e(s_0/s_1)]/(b_1-b_0). \quad (1)$$

Where S_1 and S_0 are signal values of the images at b values, b_1 and b_0, respectively, and ADC is the apparent diffusion coefficient.

Regions of Interest (ROIs) were delineated on the primary tumor and neck nodal metastases by an experienced neuroradiologist on the DW-MRI image (b = 0 s/mm^2). Before contouring the ROIs, the T1-T2-weighted images were used to determine localization and tumor extent.

Finally, a relative percentage (%) change in derived imaging metric (ADC) between pre- and ith intra-Tx week (Wk) was calculated as follows:

$$\Delta ADC\ (\%) = [(ADC_i-ADC_0)/ADC_0] \times 100. \quad (2)$$

Where ith represents intra-TX week for ADC metric value and ADC_0 represents the pre-Tx metric value.

^{18}F-FDG PET/CT: An experienced radiation oncologist matched the ROIs from the MR images with those of the PET/CT images and analyzed them qualitatively and quantitatively using the attenuation-corrected PET emission images. The ROIs were placed over the areas of focal ^{18}F-FDG uptake in both the primary tumor and neck nodal metastases. The intensity of the ^{18}F-FDG uptake in the ROIs was measured using the SUV normalized by the dilution volume[22]. The imaging data available in units of mCi per mL (mCi/mL) per voxel were decay-corrected to the time of injection and converted to SUV units.

Statistical analysis

In the present study, data was analyzed from a total of 34 multimodality imaging studies [DW-MRI (n = 24) pre-, during- (2-3 wk) and post-Tx and ^{18}F-FDG PET/CT pre- and post-Tx (n = 10)] to capture treatment response. Values were presented as mean ± SD. The mean value comparison was carried out using the Wilcoxon test. A Spearman correlation analysis was performed between SUV and ADC metric values, which we used to report the correlation and P-values. These correlations were reported using the standard guidelines[23] in which an absolute correlation of < 0.3 was considered weak, 0.3-0.5 was considered moderate and 0.5-1.0 was considered strong. The significance level was set at $P \leqslant 0.05$. All data analysis was performed using the R software/environment, an open source project that is distributed under the GNU General Public License[24].

RESULTS

All 6 patients were untreated at the first time point of multimodality imaging, had biopsy-proven SCC, and were HPV-. Among the 6 patients, a total of 11 neck nodal metastases and 5 primary tumors were analyzed (3 patients had more than one node and 1 patient had an unknown primary tumor site). Patients were grouped as follows based on clinical outcome: NED = 1, AWD = 3, and DOD = 2 (Table 1). A total of 34 multimodality imaging studies [DW-MRI (n = 24) and ^{18}F-FDG PET/

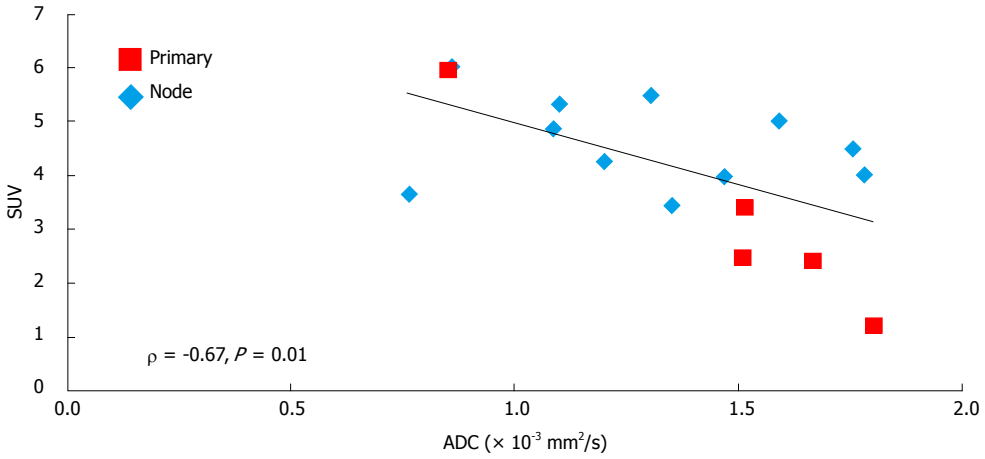

Figure 2 Relationship between pre-Tx mean standardized uptake value and pre-Tx mean apparent diffusion coefficient showing a significant strong negative inverse correlation. SUV: Standardized uptake value; ADC: Apparent diffusion coefficient.

Table 2 Apparent diffusion coefficient metric values for human papillomavirus negative head and neck squamous cell carcinoma patients who were classified based on survival as dead of disease, alive with disease and no evidence of disease before, during and post- radiotherapy

MRI	DOD ADC mean (× 10^{-3} mm^2/s)		AWD ADC mean (× 10^{-3} mm^2/s)		NED ADC mean (× 10^{-3} mm^2/s)	
	Primary	Node	Primary	Node	Primary	Node
Pre-Tx	1.51 ± 0.36	1.43 ± 0.58	1.66 ± 0.41	1.26 ± 0.19	0.85 ± 0.27	0.86 ± 0.20
During Tx (2-3 wk)	1.92 ± 0.33	1.54 ± 0.11	2.12 ± 0.38	1.41 ± 0.38	1.49 ± 0.13	1.39 ± 0.08
Post-Tx	No primary	0.98 ± 0.29	No primary	1.93 ± 0.22	No primary	No node

MRI: Magnetic resonance imaging; ADC: Apparent diffusion coefficient; AWD: Alive with disease; DOC: Dead of other causes; DOD: Dead of disease; NED: No evidence of disease.

CT (n = 10)] were analyzed to capture RT response. The results showed a significantly strong negative correlation (ρ = -0.67, P = 0.01) between the pre-Tx mean SUV and the pre-Tx mean ADC for the 11 lymph nodes and 5 primary tumors (Figure 2).

A summary of the ADC mean for pre-Tx and during-Tx (2nd and 3rd weeks data were combined) from the three different survival groups as DOD, AWD and NED is shown in Table 2. For a single patient who was NED at the last clinical follow-up, the MRI and the ^{18}F-FDG PET/CT post-treatment showed no evidence of disease at the primary tumor site and neck nodal metastases. Figure 3 shows the DW-MRI and ^{18}F-FDG PET/CT images from a patient who was NED. The ADC values (mean ± SD) for the ROI drawn on the primary tumor were 0.85 ± 0.27 × 10^{-3} mm^2/s, 1.49 ± 0.13 × 10^{-3} mm^2/s for pre-Tx and Wk2-3 Tx, respectively. The ADC values for the ROIs in neck nodal metastases were as follows 0.86 ± 0.20 × 10^{-3} mm^2/s, 1.39 ± 0.08 × 10^{-3} mm^2/s for pre-Tx and Wk2-3 Tx (Table 2). Pre-Tx SUV (mean ± SD) values for primary tumor and neck nodal metastases were 5.99 ± 0.61 and 6.06 ± 0.49, respectively.

Three patients were AWD on the last clinical follow-up, and 1 patient had an unknown primary tumor site. Both, MRI and ^{18}F-FDG PET/CT post-treatment showed no evidence of disease at the primary tumor site; however the neck nodal metastases were still present. Figure 4 shows the DW-MRI and ^{18}F-FDG PET/CT images from a patient who was AWD. The ADC values (mean ± SD) for the primary tumors were 1.66 ± 0.41 × 10^{-3} mm^2/s, 2.12 ± 0.38 × 10^{-3} mm^2/s for pre-Tx and Wk2-3 Tx, respectively. The ADC values for the neck nodal metastases were 1.26 ± 0.19 × 10^{-3} mm^2/s, 1.41 ± 0.38 × 10^{-3} mm^2/s, and 1.93 ± 0.22 × 10^{-3} mm^2/s for pre-Tx, Wk2-3 Tx and post-Tx, respectively (Table 2). The SUV mean pre-Tx values for the primary tumor and neck nodal metastases were 1.84 ± 0.83 and 4.85 ± 0.75, respectively.

The two patients who were DOD died 2 mo and 6 mo post-Tx. Figure 5 shows the DW-MRI and ^{18}F-FDG PET/CT images from a patient who was DOD. The ADC values (mean ± SD) for the primary tumor were 1.51 ± 0.36 × 10^{-3} mm^2/s and 1.92 ± 0.33 × 10^{-3} mm^2/s for pre-Tx and Wk2-3 Tx, respectively. The ADC values for the neck nodal metastases were 1.43 ± 0.58 × 10^{-3} mm^2/s, 1.54 ± 0.11 × 10^{-3} mm^2/s, and 0.98 ± 0.29 × 10^{-3} mm^2/s for pre-Tx, Wk2-3 Tx and post-Tx, respectively (Table 2). The SUV mean pre-Tx values for the primary tumor and neck nodal metastases were 2.98 ± 0.66 and 3.93 ± 0.45, respectively.

The ΔADC (%) between pre- and Wk2-3 Tx for primary tumors and neck nodal metastases were as follows: 75.4% and 61.6%, respectively, for the patient with NED, 27.5% and 32.7%, respectively, for those

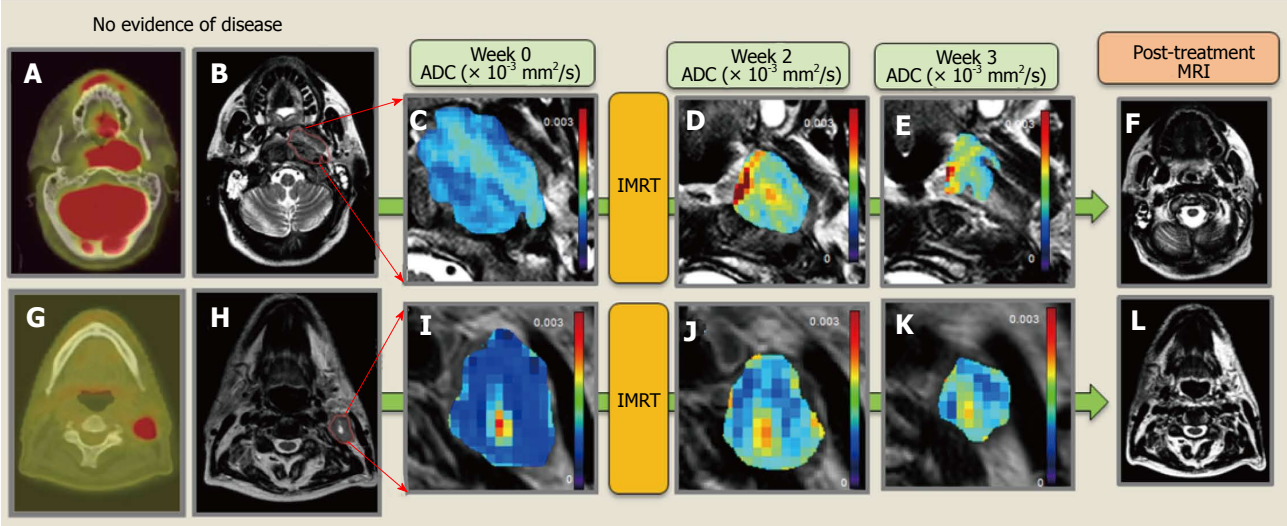

Figure 3 Representative no evidence of disease patient. A and G: Pre-Tx PET/CT of the primary tumor and a neck nodal metastasis; B and H: Primary tumor and representative neck nodal metastasis contoured over a T2-W MRI; C and I: Pre-Tx ADC map overlaid on T2-W MRI; D and J: Wk2-Tx ADC map overlaid on T2-W; E and K: Wk3-Tx ADC map overlaid on T2-W; F and L: T2-W MRI post-Tx with no evidence of primary tumor and neck nodal metastases. PET/CT: Positron emission tomography/computed tomography; MRI: Magnetic resonance imaging; ADC: Apparent diffusion coefficient; IMRT: Intensity modulated radiation therapy.

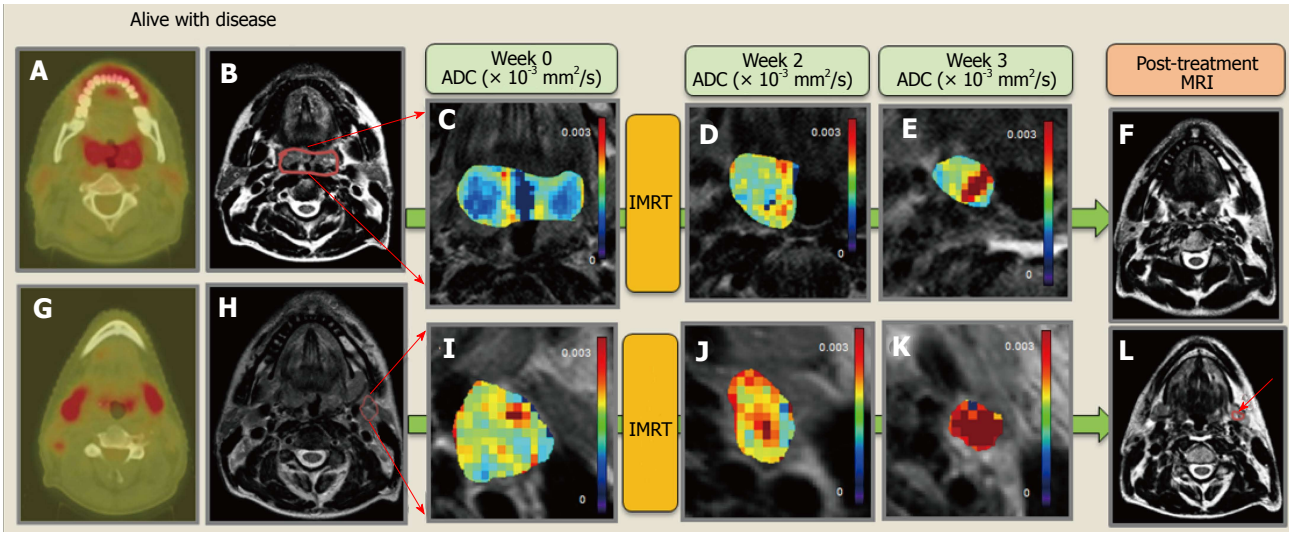

Figure 4 Representative alive with disease patient. A and G: pre-Tx PET/CT of the primary tumor and two neck nodal metastases; B and H: Primary tumor and representative neck nodal metastasis contoured over a T2-W MRI; C and I: Pre-Tx ADC map overlaid on T2-W MRI; D and J: Wk2-Tx ADC map overlaid on T2-W; E and K: Wk3-Tx ADC map overlaid on T2-W; F and L: T2-W MRI post-Tx with no evidence of primary tumor but with presence of neck nodal metastasis. PET/CT: Positron emission tomography/computed tomography; MRI: Magnetic resonance imaging; ADC: Apparent diffusion coefficient; IMRT: Intensity modulated radiation therapy.

patients who were AWD, and 26.9% and 7.31%, respectively, for those who were DOD.

DISCUSSION

This prospective study is the first in Spain conducted in support of integrating functional imaging in a RT setting. We evaluated multimodality imaging in HPV-HNSCC patients for both primary and neck nodal metastases. Specifically, we observed that pretreatment tumor cellularity is inversely proportional to glucose metabolism in these tumors, which was consistent with the previous literature[15,25,26]. The survival status and functional metrics show different % change in ΔADC for the NED, AWD, and DOD survival groups, which would need to be validated in larger patient population studies.

HNSCC is one of the major types of cancer that can be linked to alcohol consumption and tobacco smoking. It typically originates from the mucosal epithelia of the oral cavity, pharynx and larynx[27]. In oropharyngeal SCC, HPV status is an independent prognostic factor for both overall survival and progression-free survival, which is consistent with the hypothesis that HPV+ and HPV- tumors are distinct and have different causes, risk-factor profiles, and survival outcomes[28]. HPV- tumors continue to have poor outcomes compared to

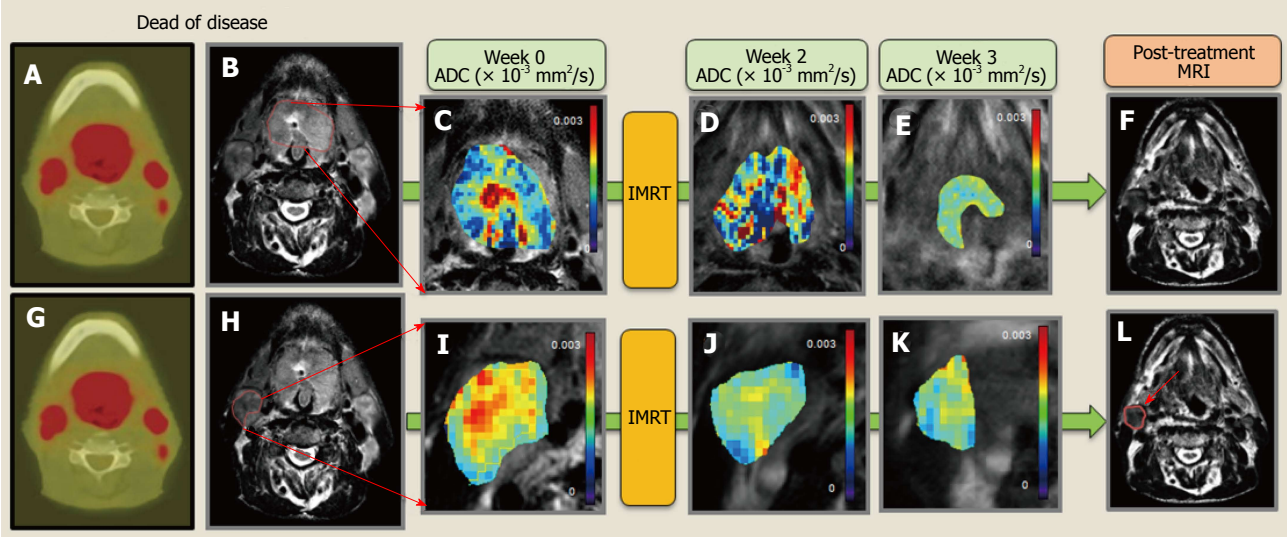

Figure 5 Representative dead of disease patient. A and G: Pre-Tx PET/CT of the primary tumor and three neck nodal metastases; B and H: Primary tumor and representative neck nodal metastasis contoured over a T2-W MRI; C and I: Pre-Tx ADC map overlaid on T2-W MRI; D and J: Wk2-Tx ADC map overlaid on T2-W; E and K: Wk3-Tx ADC map overlaid on T2-W; F and L: T2-W MRI post-Tx with no evidence of primary tumor but with presence of neck nodal metastasis. PET/CT: Positron emission tomography/computed tomography; MRI: Magnetic resonance imaging; ADC: Apparent diffusion coefficient; IMRT: Intensity modulated radiation therapy.

their HPV+ counterparts[28]. Future clinical trials should be designed specifically for patients with HPV+ or HPV- HNSCC using appropriate, validated quantitative imaging biomarkers. As there is very scarce imaging literature on HPV+ or HPV- alone, it raises an urgent need to study these cohorts independently and assess the value of multimodality imaging for better cancer patient management.

In recent years, studies by Razek have shown that ADC metric has a prognostic value in HNSCC[29-31]. They reported a mean ADC value in nasopharyngeal carcinoma (NPC) of 0.99 ± 0.11 × 10^{-3} mm^2/s. The ADC value in this study also correlated inversely with tumor volume[29]. In a separate study by the same group, it was reported that the mean ADC value of residual or recurrent lesions (1.17 ± 0.33 × 10^{-3} mm^2/s) was less than that observed in post-therapeutic changes (2.07 ± 0.25 × 10^{-3} mm^2/s)[30]. They also showed that ADC values with metabolic ratio (Ch/Cr) obtained from 1H-MRS are well correlated with several prognostic parameters of HNSCC[31].

The use of multimodality imaging (^{18}F-FDG PET/CT, DW-MRI, DCE-MRI) in general HNSCC populations for assessing both the association between the quantitative imaging biomarkers obtained from each imaging technique and their combined or respective roles in prognosis and/or prediction of outcome[8,25,32,33]. The major technical challenges in IMRT persist in the use of functional images for treatment, one of which includes the identification of a reproducible, RT-compatible patient positioning setup that is consistent between functional techniques and RT. All patients in the present study were in a supine position and fixed in place with the same immobilization system that was used during the RT treatment planning and delivery. A thermoplastic mask, head support, and flat table were used to try to minimize distortion and to improve the registration process between the different imaging modalities. The head support and flat table were adapted to MRI and PET/CT. This reproducible positioning addressed one of the big hurdles in the acquisition of multimodality images that may be used for adaptive RT in the future[34,35]. Dirix *et al*[36] designed a feasibility, prospective, multimodality imaging study with this prerequisite in mind, recruiting HNSCC patients for dose painting in RT. A pilot study by Subesinghe *et al*[37] emphasized the importance of reproducing the positioning for assessing early RT treatment response.

^{18}F-FDG PET/CT and DW-MRI have been the focus of numerous studies in general HNSCC cohorts to determine correlation, if any, between SUV and ADC values, with variable results. SUV and ADC remain exploratory imaging metrics yet to be fully explored and understood in HPV-HNSCC patients. A study by Varoquax *et al*[38] involving 24 primary and 10 recurrent HNSCC showed no significant correlation between SUV values (SUV_{max}, SUV_{mean} or SUV_{min}) and ADC values (ADC_{max}, ADC_{mean} or ADC_{min}), nor did Choi *et al*[39] find significant correlation between SUV_{mean} and ADC_{mean} in 47 primary HNSCC. Rather, Nakajo *et al*[15] found significant negative correlation between SUV_{max} and ADC_{mean} in a study of 28 primary HNSCC tumors and Nakamatsu *et al*[26] demonstrated significant negative correlation in 41 neck nodal metastases between SUV values (SUV_{max}, SUV_{mean}) and ADC values (ADC_{mean}, ADC_{min}). In our study, similar results were obtained from a total of 11 neck nodal metastases and 5 primary HPV- HNSCC showing a significant strong negative correlation between the ADC_{mean} and SUV_{mean} pre-Tx (ρ = -0.67, P = 0.01). Further validation of the correlations with larger patient populations is needed, but was beyond the scope of this

study. Preda *et al*[40] concluded in a study with 57 HNSCC primary tumors that "the combination of SUV_{max} and ADC_{min} improves the prognostic role of the two separate parameters".

The present study showed an increase in ΔADC Wk_{2-3} for the HPV- patient with NED in comparison with the DOD and AWD HPV- patients in both primary tumor and neck nodal metastases, in agreement with above-mentioned studies. Also, the pre-Tx ADC values of the primary tumor and neck nodal metastases for NED is lower than in the group of AWD and DOD, showing that lower pre-Tx ADC values are related to a good response to treatment and are consistent with the previous literature[9,41].

The % change in ΔADC for primary tumor and neck nodal metastases depict the different Tx responses, suggesting the possibility of identifying HPV- patients with poor prognosis at an early stage to individualize and adapt RT treatment (*i.e.*, through dose-escalation). Vandecaveye *et al*[42] showed in neck nodal metastases and primary tumors that ΔADC (Week 2 and Week 4 during CRT) was significantly lower ($P < 0.0001$) in lesions with recurrence than in lesions with a complete response.

Individualization of treatment is especially important in the subgroup of HPV- patients who were part of this study. A limitation of the study was that there were a relatively small number of HPV- patients as the recruitment was highly selective in Spain. However, we felt that this selectivity was justified given that these subtypes of HPV- patients are the ones who have poor prognoses in HNSCC[28]. The initial results need to be addressed through validation in future studies.

Our study offers insight on how to manage and understand valuable quantitative imaging biomarkers, such as SUV and ADC for HPV- HNSCC, with the objective of integrating them into the development of biological adaptive RT in the future.

These results are preliminary in nature and are indicative, and not definitive, trends rendered by the imaging metrics due to the small sample size of HPV- HNSCC patients in a Meixoeiro Hospital of Vigo Experience.

ACKNOWLEDGMENTS

The authors offer their sincerest thanks to patients who volunteered to participate in this study. Our sincerest thanks to Mr. James Keller, Editor, Department of Medical Physics, Memorial Sloan Kettering Cancer Center for his help in editing this paper. We must be grateful for the exchange program AAPM-SEFM for facilitating the first author's visit to Memorial Sloan Kettering Cancer Center. We thank the National Health Institute of Spain for supporting this work through the ISCIII Grant PI11/02035, DTS14/00018, BIOCAPS, and the Galician Government through the project CN 2012/260 "Consolidation Research Units: AtlantTIC". This research was also funded in part through the NIH/NCI Cancer Center Support Grant P30 CA008748.

COMMENTS

Background

Human papillomavirus (HPV) negative (-) head and neck squamous cell carcinoma (HNSCC) patients have poor outcomes compared with HPV-positive (HPV+) cancers. Individualization of radiotherapy is especially important in the subgroup of HPV- patients and imaging metrics derived from multimodality imaging can be critical for its implementation.

Research frontiers

In an effort to perform biologically guided adaptive radiotherapy, it is critical to understand how different functional imaging techniques interact and potentially complement each other.

Innovations and breakthroughs

Multimodality imaging in HPV- HNSCC suggests that tumor cell density is inversely proportional to glucose metabolism in a Meixoeiro Hospital of Vigo Experience. These results are promising and need to be validated in larger populations.

Applications

Diffusion-weighted magnetic resonance imaging and ^{18}F-labeled fluoro-deoxyglucose positron emission tomography/computed tomography are two valuable imaging techniques that may help build the framework for adaptive radiotherapy based on functional images in future clinical trials by investigating tumor cellularity and glucose metabolism before, during and after RT in HPV- HNSCC.

Terminology

^{18}F-FDG: Fluorine-18 fludeoxyglucose; ADC: Apparent diffusion coefficient; AWD: Alive with disease; DOC: Dead of other causes; DOD: Dead of disease; DW-MRI: Diffusion-weighted magnetic resonance imaging; HNC: Head and neck cancer; HNSCC: Head and neck squamous cell carcinoma; HPV-: Human papillomavirus negative; HPV+: Human papillomavirus positive; IMRT: Intensity modulated radiation therapy; MRI: Magnetic resonance imaging; NED: No evidence of disease; PET/CT: Positron emission tomography/computed tomography; ROI: Region of interest; RT: Radiotherapy.

Peer-review

This is a good paper.

REFERENCES

1 **Galceran**. Europa: Estimaciones de la incidencia y la supervivencia del cáncer en Espa-a y su situación en Europa, 2014
2 **Sanderson RJ**, Ironside JA. Squamous cell carcinomas of the head and neck. *BMJ* 2002; **325**: 822-827 [PMID: 12376446 DOI: 10.1136/bmj.325.7368.822]
3 **Seijas-Tamayo R**, Fernández-Mateos J, Adansa Klain JC, Mesía R, Pastor Borgoñón M, Pérez-Ruiz E, Vázquez Fernández S, Salvador Coloma C, Rueda Domínguez A, Taberna M, Martínez-Trufero J, Bonfill Abella T, Vázquez Estévez S, Pollán M, Del Barco Morillo E, Cruz-Hernández JJ. Epidemiological characteristics of a Spanish cohort of patients diagnosed with squamous cell carcinoma of head and neck: distribution of risk factors by tumor location. *Clin Transl Oncol* 2016; **18**: 1114-1122 [PMID: 27112939 DOI: 10.1007/s12094-016-1493-1]
4 **Fakhry C**, Westra WH, Li S, Cmelak A, Ridge JA, Pinto H, Forastiere A, Gillison ML. Improved survival of patients with human papillomavirus-positive head and neck squamous cell carcinoma in a prospective clinical trial. *J Natl Cancer Inst* 2008; **100**: 261-269 [PMID: 18270337 DOI: 10.1093/jnci/djn011]
5 **Jansen JF**, Schöder H, Lee NY, Stambuk HE, Wang Y, Fury MG, Patel SG, Pfister DG, Shah JP, Koutcher JA, Shukla-Dave A. Tumor metabolism and perfusion in head and neck squamous cell carcinoma:

pretreatment multimodality imaging with 1H magnetic resonance spectroscopy, dynamic contrast-enhanced MRI, and [18F]FDG-PET. *Int J Radiat Oncol Biol Phys* 2012; **82**: 299-307 [PMID: 21236594 DOI: 10.1016/j.ijrobp.2010.11.022]

6 **Padhani AR**, Liu G, Koh DM, Chenevert TL, Thoeny HC, Takahara T, Dzik-Jurasz A, Ross BD, Van Cauteren M, Collins D, Hammoud DA, Rustin GJ, Taouli B, Choyke PL. Diffusion-weighted magnetic resonance imaging as a cancer biomarker: consensus and recommendations. *Neoplasia* 2009; **11**: 102-125 [PMID: 19186405 DOI: 10.1593/neo.81328]

7 **Chenevert TL**, Stegman LD, Taylor JM, Robertson PL, Greenberg HS, Rehemtulla A, Ross BD. Diffusion magnetic resonance imaging: an early surrogate marker of therapeutic efficacy in brain tumors. *J Natl Cancer Inst* 2000; **92**: 2029-2036 [PMID: 11121466 DOI: 10.1093/jnci/92.24.2029]

8 **Ng SH**, Liao CT, Lin CY, Chan SC, Lin YC, Yen TC, Chang JT, Ko SF, Fan KH, Wang HM, Yang LY, Wang JJ. Dynamic contrast-enhanced MRI, diffusion-weighted MRI and (18)F-FDG PET/CT for the prediction of survival in oropharyngeal or hypopharyngeal squamous cell carcinoma treated with chemoradiation. *Eur Radiol* 2016; **26**: 4162-4172 [PMID: 26911889 DOI: 10.1007/s00330-016-4276-8]

9 **Kim S**, Loevner L, Quon H, Sherman E, Weinstein G, Kilger A, Poptani H. Diffusion-weighted magnetic resonance imaging for predicting and detecting early response to chemoradiation therapy of squamous cell carcinomas of the head and neck. *Clin Cancer Res* 2009; **15**: 986-994 [PMID: 19188170 DOI: 10.1158/1078-0432.CCR-08-1287]

10 **Vandecaveye V**, Dirix P, De Keyzer F, Op de Beeck K, Vander Poorten V, Hauben E, Lambrecht M, Nuyts S, Hermans R. Diffusion-weighted magnetic resonance imaging early after chemoradiotherapy to monitor treatment response in head-and-neck squamous cell carcinoma. *Int J Radiat Oncol Biol Phys* 2012; **82**: 1098-1107 [PMID: 21514067 DOI: 10.1016/j.ijrobp.2011.02.044]

11 **Schöder H**, Fury M, Lee N, Kraus D. PET monitoring of therapy response in head and neck squamous cell carcinoma. *J Nucl Med* 2009; **50** Suppl 1: 74S-88S [PMID: 19380408 DOI: 10.2967/jnumed.108.057208]

12 **Ong SC**, Schöder H, Lee NY, Patel SG, Carlson D, Fury M, Pfister DG, Shah JP, Larson SM, Kraus DH. Clinical utility of 18F-FDG PET/CT in assessing the neck after concurrent chemoradiotherapy for Locoregional advanced head and neck cancer. *J Nucl Med* 2008; **49**: 532-540 [PMID: 18344440 DOI: 10.2967/jnumed.107.044792]

13 **Wong RJ**, Lin DT, Schöder H, Patel SG, Gonen M, Wolden S, Pfister DG, Shah JP, Larson SM, Kraus DH. Diagnostic and prognostic value of [(18)F]fluorodeoxyglucose positron emission tomography for recurrent head and neck squamous cell carcinoma. *J Clin Oncol* 2002; **20**: 4199-4208 [PMID: 12377963 DOI: 10.1200/JCO.2002.02.590]

14 **Schwartz DL**, Rajendran J, Yueh B, Coltrera MD, Leblanc M, Eary J, Krohn K. FDG-PET prediction of head and neck squamous cell cancer outcomes. *Arch Otolaryngol Head Neck Surg* 2004; **130**: 1361-1367 [PMID: 15611393 DOI: 10.1001/archotol.130.12.1361]

15 **Nakajo M**, Nakajo M, Kajiya Y, Tani A, Kamiyama T, Yonekura R, Fukukura Y, Matsuzaki T, Nishimoto K, Nomoto M, Koriyama C. FDG PET/CT and diffusion-weighted imaging of head and neck squamous cell carcinoma: comparison of prognostic significance between primary tumor standardized uptake value and apparent diffusion coefficient. *Clin Nucl Med* 2012; **37**: 475-480 [PMID: 22475897 DOI: 10.1097/RLU.0b013e318248524a]

16 **Min M**, Lee MT, Lin P, Holloway L, Wijesekera Dj, Gooneratne D, Rai R, Xuan W, Fowler A, Forstner D, Liney G. Assessment of serial multi-parametric functional MRI (diffusion-weighted imaging and R2*) with (18)F-FDG-PET in patients with head and neck cancer treated with radiation therapy. *Br J Radiol* 2016; **89**: 20150530 [PMID: 26648404 DOI: 10.1259/bjr.20150530]

17 **Goodyear MD**, Krleza-Jeric K, Lemmens T. The Declaration of Helsinki. *BMJ* 2007; **335**: 624-625 [PMID: 17901471 DOI: 10.1136/bmj.39339.610000.BE]

18 **Bockmühl U**, Ishwad CS, Ferrell RE, Gollin SM. Association of 8p23 deletions with poor survival in head and neck cancer. *Otolaryngol Head Neck Surg* 2001; **124**: 451-455 [PMID: 11283506 DOI: 10.1067/mhn.2001.114794]

19 **Landesa-Vazquez I**, Alba-Castro JL, Mera-Iglesias M, Aramburu-Nunez D, Lopez-Medina A, Munoz-Garzon V. ARTFIBio: A Cross-Platform Image Registration Tool for Tumor Response Quantification in Head and Neck Cancer. *Ieee-Embs International Conference on Biomedical and Health Informatics* (Bhi) 2014: 149-152 [DOI: 10.1109/BHI.2014.6864326]

20 **Mattes D**, Haynor DR, Vesselle H, Lewellen TK, Eubank W. Nonrigid multimodality image registration. *P Soc Photo-Opt Ins* 2001; **2**: 1609-1620 [DOI: 10.1117/12.431046]

21 **Stejskal EO**, Tanner JE. Spin Diffusion Measurements: Spin Echoes in the Presence of a Time-Dependent Field Gradient. *J Chem Phys* 1965; **42**: 288-292 [DOI: 10.1063/1.1695690]

22 **IAEA**. Quantitative Nuclear Medicine Imaging: Concepts, Requirements and Methods. Austria: IAEA Library, 2014

23 **Cohen J**. The statistical power of abnormal-social psychological research: a review. *J Abnorm Soc Psychol* 1962; **65**: 145-153 [PMID: 13880271 DOI: 10.1037/h0045186]

24 **R Project**. GNU Operating System. Available from: URL: http://www.gnu.org/licenses/gpl.html

25 **Gawlitza M**, Purz S, Kubiessa K, Boehm A, Barthel H, Kluge R, Kahn T, Sabri O, Stumpp P. In Vivo Correlation of Glucose Metabolism, Cell Density and Microcirculatory Parameters in Patients with Head and Neck Cancer: Initial Results Using Simultaneous PET/MRI. *PLoS One* 2015; **10**: e0134749 [PMID: 26270054 DOI: 10.1371/journal.pone.0134749]

26 **Nakamatsu S**, Matsusue E, Miyoshi H, Kakite S, Kaminou T, Ogawa T. Correlation of apparent diffusion coefficients measured by diffusion-weighted MR imaging and standardized uptake values from FDG PET/CT in metastatic neck lymph nodes of head and neck squamous cell carcinomas. *Clin Imaging* 2012; **36**: 90-97 [PMID: 22370129 DOI: 10.1016/j.clinimag.2011.05.002]

27 **Jemal A**, Siegel R, Xu J, Ward E. Cancer statistics, 2010. *CA Cancer J Clin* 2010; **60**: 277-300 [PMID: 20610543 DOI: 10.3322/caac.20073]

28 **Ang KK**, Harris J, Wheeler R, Weber R, Rosenthal DI, Nguyen-Tân PF, Westra WH, Chung CH, Jordan RC, Lu C, Kim H, Axelrod R, Silverman CC, Redmond KP, Gillison ML. Human papillomavirus and survival of patients with oropharyngeal cancer. *N Engl J Med* 2010; **363**: 24-35 [PMID: 20530316 DOI: 10.1056/NEJMoa0912217]

29 **Abdel Razek AA**, Kamal E. Nasopharyngeal carcinoma: correlation of apparent diffusion coefficient value with prognostic parameters. *La Radiologia medica* 2013; **118**: 534-539 [PMID: 23090251 DOI: 10.1007/s11547-012-0890-x]

30 **Abdel Razek AA**, Kandeel AY, Soliman N, El-shenshawy HM, Kamel Y, Nada N, Denewar A. Role of diffusion-weighted echo-planar MR imaging in differentiation of residual or recurrent head and neck tumors and posttreatment changes. *AJNR American journal of neuroradiology* 2007; **28**: 1146-1152 [PMID: 17569975 DOI: 10.3174/ajnr.A0491]

31 **Razek AA**, Nada N. Correlation of Choline/Creatine and Apparent Diffusion Coefficient values with the prognostic parameters of Head and Neck Squamous Cell Carcinoma. *NMR in biomedicine* 2016; **29**: 483-489 [PMID: 26867020 DOI: 10.1002/nbm.3472]

32 **Han M**, Kim SY, Lee SJ, Choi JW. The Correlations Between MRI Perfusion, Diffusion Parameters, and 18F-FDG PET Metabolic Parameters in Primary Head-and-Neck Cancer: A Cross-Sectional Analysis in Single Institute. *Medicine* (Baltimore) 2015; **94**: e2141 [PMID: 26632740 DOI: 10.1097/MD.0000000000002141]

33 **Shukla-Dave A**, Lee NY, Jansen JF, Thaler HT, Stambuk HE, Fury MG, Patel SG, Moreira AL, Sherman E, Karimi S, Wang Y, Kraus D, Shah JP, Pfister DG, Koutcher JA. Dynamic contrast-enhanced magnetic resonance imaging as a predictor of outcome in head-and-neck squamous cell carcinoma patients with nodal metastases. Int *J Radiat Oncol Biol Phys* 2012; **82**: 1837-1844 [PMID: 21601373 DOI: 10.1016/j.ijrobp.2011.03.006]

34 **van der Heide UA**, Houweling AC, Groenendaal G, Beets-Tan RG, Lambin P. Functional MRI for radiotherapy dose painting. *Magn Reson Imaging* 2012; **30**: 1216-1223 [PMID: 22770686 DOI:

10.1016/j.mri.2012.04.010]

35 **Thorwarth D**, Beyer T, Boellaard R, de Ruysscher D, Grgic A, Lee JA, Pietrzyk U, Sattler B, Schaefer A, van Elmpt W, Vogel W, Oyen WJ, Nestle U. Integration of FDG-PET/CT into external beam radiation therapy planning: technical aspects and recommendations on methodological approaches. *Nuklearmedizin* 2012; **51**: 140-153 [PMID: 22473130 DOI: 10.3413/Nukmed-0455-11-12]

36 **Dirix P**, Vandecaveye V, De Keyzer F, Stroobants S, Hermans R, Nuyts S. Dose painting in radiotherapy for head and neck squamous cell carcinoma: value of repeated functional imaging with (18)F-FDG PET, (18)F-fluoromisonidazole PET, diffusion-weighted MRI, and dynamic contrast-enhanced MRI. *J Nucl Med* 2009; **50**: 1020-1027 [PMID: 19525447 DOI: 10.2967/jnumed.109.062638]

37 **Subesinghe M**, Scarsbrook AF, Sourbron S, Wilson DJ, McDermott G, Speight R, Roberts N, Carey B, Forrester R, Gopal SV, Sykes JR, Prestwich RJ. Alterations in anatomic and functional imaging parameters with repeated FDG PET-CT and MRI during radiotherapy for head and neck cancer: a pilot study. *BMC Cancer* 2015; **15**: 137 [PMID: 25885109 DOI: 10.1186/s12885-015-1154-8]

38 **Varoquaux A**, Rager O, Lovblad KO, Masterson K, Dulguerov P, Ratib O, Becker CD, Becker M. Functional imaging of head and neck squamous cell carcinoma with diffusion-weighted MRI and FDG PET/CT: quantitative analysis of ADC and SUV. *Eur J Nucl Med Mol Imaging* 2013; **40**: 842-852 [PMID: 23436068 DOI: 10.1007/s00259-013-2351-9]

39 **Choi SH**, Paeng JC, Sohn CH, Pagsisihan JR, Kim YJ, Kim KG, Jang JY, Yun TJ, Kim JH, Han MH, Chang KH. Correlation of 18F-FDG uptake with apparent diffusion coefficient ratio measured on standard and high b value diffusion MRI in head and neck cancer. *J Nucl Med* 2011; **52**: 1056-1062 [PMID: 21680692 DOI: 10.2967/jnumed.111.089334]

40 **Preda L**, Conte G, Bonello L, Giannitto C, Travaini LL, Raimondi S, Summers PE, Mohssen A, Alterio D, Cossu Rocca M, Grana C, Ruju F, Bellomi M. Combining standardized uptake value of FDG-PET and apparent diffusion coefficient of DW-MRI improves risk stratification in head and neck squamous cell carcinoma. *Eur Radiol* 2016 [PMID: 26965504 DOI: 10.1007/s00330-016-4284-8]

41 **Hatakenaka M**, Nakamura K, Yabuuchi H, Shioyama Y, Matsuo Y, Kamitani T, Yonezawa M, Yoshiura T, Nakashima T, Mori M, Honda H. Apparent diffusion coefficient is a prognostic factor of head and neck squamous cell carcinoma treated with radiotherapy. *Jpn J Radiol* 2014; **32**: 80-89 [PMID: 24408077 DOI: 10.1007/s11604-013-0272-y]

42 **Vandecaveye V**, Dirix P, De Keyzer F, de Beeck KO, Vander Poorten V, Roebben I, Nuyts S, Hermans R. Predictive value of diffusion-weighted magnetic resonance imaging during chemoradiotherapy for head and neck squamous cell carcinoma. *Eur Radiol* 2010; **20**: 1703-1714 [PMID: 20179939 DOI: 10.1007/s00330-010-1734-6]

P- Reviewer: Razek AAKA, Xiao NH **S- Editor**: Ji FF **L- Editor**: A
E- Editor: Lu YJ

Published by **Baishideng Publishing Group Inc**
8226 Regency Drive, Pleasanton, CA 94588, USA
Telephone: +1-925-223-8242
Fax: +1-925-223-8243
E-mail: bpgoffice@wjgnet.com
Help Desk: http://www.wjgnet.com/esps/helpdesk.aspx
http://www.wjgnet.com